Transgenic Dendra2::tau expression allows *in vivo* monitoring of tau proteostasis in *C. elegans*

Marina Han[1,2], Aleen Saxton[3], Heather Currey[3], Sarah M. Waldherr[2,3], Nicole F. Liachko[2,3], and Brian C. Kraemer[2,3,4,5,*]

[1]Graduate Program in Neuroscience, University of Washington, Seattle, WA 98195, USA
[2]Division of Gerontology and Geriatric Medicine, Department of Medicine, University of Washington, Seattle, WA 98104, USA
[3]Geriatrics Research Education and Clinical Center, Veterans Affairs Puget Sound Health Care System, Seattle, WA 98108, USA
[4]Department of Psychiatry and Behavioral Sciences, University of Washington, Seattle, WA 98195, USA
[5]Department of Laboratory Medicine and Pathology, University of Washington, Seattle, WA 98195, USA

[*]To whom correspondence should be addressed at:
Seattle Veterans Affairs Puget Sound Health Care System
S182, 1660 South Columbian Way, Seattle, WA 98108
Phone (206) 277-1071 Fax (206) 764-2569
Email: kraemerb@u.washington.edu

Summary Statement

Diseases exhibiting pathological tau protein comprise the majority of dementia cases highlighting the need for new therapeutic targets; investigation of molecular tauopathy mechanisms in *C. elegans* can inform disease mechanisms.

Abstract

Protein homeostasis is perturbed in aging-related neurodegenerative diseases called tauopathies, which are pathologically characterized by aggregation of the microtubule-associated protein tau. Transgenic *Caenorhabditis elegans* serve as a powerful model organism to study tauopathy disease mechanisms, but moderating transgenic expression level has proven problematic. To study neuronal tau proteostasis, we generated a suite of transgenic

Disease Models & Mechanisms • DMM • Accepted manuscript

strains expressing low, medium, or high levels of Dendra2::tau fusion proteins by comparing integrated multicopy transgene arrays with single-copy safe-harbor locus strains generated by recombinase-mediated cassette exchange. Multicopy Dendra2::tau strains exhibit expression level-dependent neuronal dysfunction that is modifiable by known genetic suppressors or an enhancer of tauopathy. Single-copy Dendra2::tau strains lack distinguishable phenotypes on their own but enable detection of enhancer-driven neuronal dysfunction. We have employed multicopy Dendra2::tau strains in optical pulse-chase experiments measuring tau turnover *in vivo* and found Dendra2::tau turns over faster than the relatively stable Dendra2. Further, Dendra2::tau turnover is dependent on protein expression level and independent of TDP-43 co-expression. We present Dendra2::tau transgenic *C. elegans* as a novel tool for investigating molecular mechanisms of tau proteostasis.

Keywords: Tau, *C. elegans,* Alzheimer's disease, Proteostasis, Dendra2, TDP-43

Introduction

Humans become more susceptible to neurodegenerative disease with age in part due to the stress of maintaining neuronal health across a longer lifespan and the accumulation of pathological proteins (Hetz, 2021). Tauopathies are a group of age-related neurodegenerative disorders caused by pathological hyperphosphorylation and aggregation of the microtubule binding protein tau. They are clinically characterized by various manifestations of behavioral, motor, language, and memory impairments. Of the many distinct tauopathies, Alzheimer's disease (AD) accounts for 60-70% of dementia, while frontotemporal lobar degeneration (FTLD) accounts for 2.6% (Zhang *et al.*, 2022), making the treatment of these diseases a priority for dementia and aging research. Furthermore, although AD is also characterized by the accumulation of amyloid beta peptides, tau burden and not amyloid beta pathology has been shown to correlate with disease severity (Nelson *et al.*, 2012), indicating that tau-targeting therapies may be valuable in ameliorating clinical progression.

In healthy cellular physiology, tau binds to microtubules to promote their assembly and stability, thereby enabling axonal transport. A small fraction of tau localizes to dendrites, dendritic spines, and the post-synapse, where tau plays a yet undefined role in healthy synaptic function. Indeed, loss of tau leads to synaptic defects and functional impairment, while tau hyperphosphorylation and aggregation compromises short- and long-term plasticity (Ittner and Ittner, 2018). Tau also plays a role in myelination, neurogenesis, iron homeostasis, glucose

metabolism, and DNA protection (Wang and Mandelkow, 2016; Kent, Spires-Jones and Durrant, 2020). As a protein that is highly expressed in neurons, proper localization and function of tau is integral to neuronal health.

In disease, hyperphosphorylated tau dissociates from microtubules to form oligomers, and eventually accumulates as insoluble fibrils, disrupting neuronal function. Tau deposits exist mostly in the cytoplasm of neuronal and glial processes but can also be found in the nucleus. Tau can bind to RNA to form complexes in both cellular compartments, mislocalizing nuclear speckle components and disrupting microtubule dynamics (Ginsberg *et al.*, 1997; Lester *et al.*, 2021; PJ *et al.*, 2023). In primary tauopathies such as FTLD, Pick's disease (PiD), corticobasal degeneration (CBD), and progressive supranuclear palsy (PSP), mutations in the microtubule-associated protein tau (*MAPT*) gene cause changes in the protein's splicing, post-translational modifications, microtubule affinity, folding, or aggregation propensity that likely lead to the various pathological tau structures and localization observed in these diseases (Naseri *et al.*, 2019; Strang, Golde and Giasson, 2019; Gallo, Ruiz and Sánchez-Juan, 2022). In contrast, most cases of AD are sporadic with wild-type tau forming aggregates. How tau becomes pathological remains unclear, and consequently, tauopathies remain untreatable. Tau levels can be decreased by inhibiting tau production or enhancing tau degradation. The latter can be achieved by targeting mechanisms of tau protein homeostasis (proteostasis).

Normally, cellular proteostasis mechanisms activate in response to an overabundance or misfolding of protein. These mechanisms include the autophagy lysosomal pathway (ALP), ubiquitin-proteasome system (UPS), and the unfolded protein response (UPR). The ALP degrades cytosolic and membrane-enclosed proteins, particularly larger ones such as aggregates and organelles, through engulfment by phagophores that fuse with lysosomes. The UPS selectively degrades soluble proteins that have been tagged with ubiquitin. Misfolded protein accumulation in the endoplasmic reticulum or mitochondria activates the UPR, resulting in transcriptional activation of proteostasis genes. In the case of the UPR^{ER}, ER-associated degradation (ERAD) directs misfolded proteins to the proteasome but can also activate autophagy.

Proteostasis impairment is a hallmark of aging (López-Otín *et al.*, 2013; Kennedy *et al.*, 2014). Accumulation of pathological tau further compromises neuronal proteostasis mechanisms. Full-length tau is selectively degraded by the UPS, while truncated, aggregated, or soluble mutant tau is degraded by the ALP (Wang *et al.*, 2009; Dolan and Johnson, 2010; Wang and Mandelkow, 2012; Hamano *et al.*, 2021). However, tau accumulation impairs autophagosome-lysosome fusion by inhibiting expression of IST-1 that is required for ESCRT

(Endosomal Sorting Complex Required for Transport) (Feng *et al.*, 2020). In addition, acetylated tau inhibits chaperone-mediated autophagy, rerouting tau to be degraded by macroautophagy and endosomal microautophagy (Caballero *et al.*, 2021). Impairing autophagy by various mechanisms leads to increased tau secretion, enabling cell-to-cell seeding (Tang *et al.*, 2015; Chen *et al.*, 2020; Caballero *et al.*, 2021). Consequently, activating autophagy with IST-1 upregulation, trehalose, methylene blue, or mammalian target of rapamycin (mTOR) inhibitors resulted in reduction of tau levels *in vivo* and *in vitro* (Schaeffer *et al.*, 2012; Hamano *et al.*, 2021).

Abnormal levels and mislocalization of multiple UPS components correspond with phosphorylated and ubiquitinated tau pathology in human AD brains (Weng and He, 2021). For instance, AD brains exhibit increased levels of carboxyl terminus of Hsp70-interacting protein (CHIP) (Sahara *et al.*, 2005), the E3 ubiquitin ligase that ubiquitinates tau paired helical filaments, targeting it to the 26S proteasome (Mori, Kondo and Ihara, 1987; Petrucelli *et al.*, 2004). Interestingly, deletion of CHIP increases tau accumulation but not aggregation (Dickey *et al.*, 2006), likely because CHIP-mediated hyper-ubiquitination of phosphorylated tau promotes its aggregation (Petrucelli *et al.*, 2004; Kim *et al.*, 2021). Despite their ubiquitination, the proteasome fails to degrade phosphorylated or insoluble tau. Tau becomes a ubiquitin sink, blocking ubiquitin recycling and potentially obstructing the proteasome core particle (Weng and He, 2021). Rescuing proteasome function with PROTAC (Proteolysis Targeting Chimera) improves tau clearance and phenotype in AD and tauopathy mouse models (Wang *et al.*, 2021).

The relationship between tau and the UPR^{ER} remains controversial. Disease-specific brain regions of AD, PSP, and PiD brains exhibit abnormally activated UPR^{ER} (Hoozemans *et al.*, 2005, 2009; Nijholt *et al.*, 2012; Stutzbach *et al.*, 2013). Tau accumulation activates the UPR^{ER} *in vivo* by compromising ERAD (Abisambra *et al.*, 2013), and conversely ER stress results in increased tau phosphorylation (Ho *et al.*, 2012). Multiple studies have shown that UPR^{ER} activation protects against tau toxicity (Loewen and Feany, 2010; Bruch *et al.*, 2017; Waldherr *et al.*, 2019; Shin *et al.*, 2021), but understanding the exact mechanism requires further investigation. Evidenced by the multitude of disease-associated alterations in proteostasis mechanisms, tau pathology is deeply intertwined with the neuronal proteostatic network. Therefore, studying tau proteostasis is imperative for developing effective tau-targeting therapies.

We used transgenic *Caenorhabditis elegans* (*C. elegans*) to investigate molecular mechanisms of tau proteostasis. Powerful genetic tools, short lifespan, ease of imaging, a thoroughly documented connectome, and high throughput functional assays make *C. elegans*

useful for studying age-related neurodegenerative tauopathy. Transgenic *C. elegans* tauopathy models exhibit quantifiable neurological deficits mirroring the molecular and cellular features of human neuropathology: uncoordinated movement, neuronal loss, disease protein aggregation, and shortened lifespan (Kraemer *et al.*, 2003). However, most previous models do not capitalize on a key strength of the model system, which is live imaging of cellular function and protein trafficking. Further, many *C. elegans* neurodegenerative disease models utilize multicopy transgenes yielding high levels of disease protein overexpression to elicit a phenotype which presents limitations in the precision of the transgenic modelling strategy.

Here, we characterize a suite of tau transgenic strains addressing both shortcomings. We used conventional transgene arrays and recombinase-mediated cassette exchange to generate several multicopy and single-copy genomically integrated strains pan-neuronally expressing the photoconvertible protein Dendra2 fused to wild-type human tau (Dendra2::tau) as a system for monitoring tau proteostasis. Upon exposure to 405nm light, Dendra2 irreversibly converts from green to red fluorescence. Dendra2 possesses several advantages over other photoactivatable fluorescent proteins: monomeric form, high contrast photoconversion, high photostability, bright fluorescence, and low phototoxic activation (Chudakov, Lukyanov and Lukyanov, 2007). The Dendra2::tau model is a useful system for studying tau proteostasis because it allows immediate visualization of tau localization and accumulation and enables optical pulse-chase experiments to measure tau turnover *in vivo*. Since approximately 60-80% of *C. elegans* genes have an analogous human counterpart and about 42% of human disease genes have a *C. elegans* ortholog (Markaki and Tavernarakis, 2010), genetic targeting of tauopathy disease mechanisms in Dendra2::tau *C. elegans* could shed light on how those mechanisms affect tau proteostasis and could be translatable to mammalian models.

Methods

C. elegans strains and maintenance.

Worms were maintained at 20°C on nematode growth media (NGM) plates seeded with OP50 *E. coli* according to standards described by Brenner (Brenner, 1974). For protein extraction, worms were grown on NGM plates containing media with five times peptone (5X PEP), nutrient rich media for robust *C. elegans* growth, seeded with OP50 (Brenner, 1974). Transgenic strains were engineered by microinjection into the wild-type N2 strain using a Nikon Eclipse TE300 microscope (Nikon, Tokyo, Japan) and Eppendorf FemtoJet injection rig (Eppendorf, Hamburg,

Germany). Multicopy transgenic strains were generated using conventional transgenic array and genomically integrated by sub-lethal dose of UV irradiation from a Stratagene Stratalinker UV 1800 Crosslinker (Stratagene, Santa Clara, CA, USA). Single-copy Dendra2::tau strains were generated by dual-component recombinase-mediated cassette exchange (Nonet, 2020). All strains were outcrossed to N2 at least twice. Transgenic strains will be made available upon request.

Protein extraction

Protein extraction and western blotting procedures were conducted as previously described (Kow *et al.*, 2018). Briefly, to create staged populations, worms were grown at 20°C on 150 mm 5X PEP plates to generate populations for hypochlorite treatment for harvest of eggs. Harvested eggs were deposited onto 5X PEP and maintained at 20°C for three days until worms were harvested from plates using M9 buffer. Worms were pelleted by centrifugation (3000×*g* 45 s) and pellets subsequently washed three times with 5 ml M9 buffer and transferred to Eppendorf tubes. Buffer was aspirated from centrifuged worms, and pellets were snap frozen with liquid nitrogen prior to storage at −70°C.

Whole worm protein lysates were created as follows. Worm pellets were thawed on ice and weighed to determine pellet mass. SDS protein sample buffer (0.046 M Tris, 0.005 M ethylenediamine tetraacetate, 0.2 M dithiothreitol, 50% sucrose, 5% sodium dodecyl sulfate, 0.05% bromophenol blue, 1X concentration) was added to the pellets at a volume (µl) four times the pellet weight (mg). Pellets were sonicated three times, 15 s each at 30% amplitude, returning to ice in between sonication sessions. Samples were boiled at 95°C for 10 min and then centrifuged at 13,200×*g* for 1 min. Samples were returned to ice prior to gel loading.

Immunoblotting

5–10 µL of lysate was loaded into each well of a 4–15% pre-cast Criterion sodium dodecyl sulfate polyacrylamide gel electrophoresis gradient gel (catalog number 3450028, Bio-Rad, Hercules, CA, USA). Gels were run at 200 V for 60 min, after which proteins were transferred to polyvinylidene difluoride (PVDF) membranes (Bio-Rad) at 80 V for 30 min and then blocked in 5% milk in phosphate-buffered saline (PBS) directly post-transfer. Membranes were incubated with primary antibodies diluted in 5% milk-PBS block solution overnight rocking at 4°C and washed three times in PBS with 0.1% Tween (10 min each wash). They were then subjected to secondary antibody incubation for 2 hr rocking at room temperature, washed three times with

PBST and detected using chemiluminescence kit (Biorad cat. number 1705060). Blots were imaged and quantitated using LiCor Odyssey Fc 2800 (LiCor, Lincoln, NE, USA).

Motility assays

Radial assay. Assessments of *C. elegans* locomotion were carried out as previously described (Currey and Liachko, 2021). In brief, 10-15 day one adult worms were placed at the center of a 100mm 5X PEP plate. Animals were allowed to move freely for 24hrs at 20°C, and the radial distance traveled from the start point was recorded.

Swimming assay. Day one adult worms were obtained by egg lay at 20°C three days prior. Worms were moved to the assay room and allowed to acclimate to ambient room temperature for at least 30 min. One strain at a time, worms were washed from NGM plates to food-free 35mm video plates with 2 ml of M9, allowed to acclimate to M9 buffer for 10s prior to a 1min video recording. Videos were acquired using the WormLab platform (MBF Bioscience, VT, USA). After videos were taken, worm movement behavior was analyzed using the WormTracker software (MBF BioScience). Body bends from the mid-point body location of each worm tracked were counted. The total number of body bends was divided by the track length to give the frequency of body bends per second.

Imaging

Unless otherwise specified, day one adult worms were mounted on a 4% agarose gel pad in 50-500mM sodium azide solution and cover slip fixed using nail polish and/or molten petroleum jelly. Worms were imaged on a Nikon A1R confocal microscope using 40x oil, 60x oil, or 100x oil immersion objective (Nikon USA, Melville, NY). Representative images are maximum intensity projections of z-stack images. Analysis was performed using ImageJ Java (Schneider, Rasband and Eliceiri, 2012). Corresponding worm diagrams were generated using BioRender (Toronto, ON, CA). Representative images in Fig 5, Fig 7, and Fig S3 were adjusted with +40% contrast and +40% brightness to enhance visibility.

Dendra2 photoconversion

A 405nm wavelength lamp positioned 8cm above the bench was used to photoconvert a single 35mm unseeded plate of day one adult worms at a time for 8 minutes to achieve maximum photoconversion while minimizing phototoxicity. Non-photoconverted Dendra2::tau and Dendra2 strains were prepared and imaged alongside photoconverted strains to establish baseline green

fluorescence intensity without photoconversion. 61-step z-stack images centered and focused on the grinder at 100x magnification were acquired on a Nikon A1R confocal microscope (Nikon, Tokyo, Japan). Non-photoconverted green Dendra2 and Dendra2::tau were imaged with the 488nm laser, while the photoconverted red Dendra2 and Dendra2::tau were imaged with the 561nm laser. Whole image fluorescence intensity of each maximum intensity projection in the green (488nm) and red (561nm) channels were quantified using ImageJ for the Dendra2::tau Tg M5 and Dendra2-only photoconversion experiment. To exclude gut autofluorescence detected by stronger laser power required for acquisition of the double copy Dendra2::tau and Tg M5 strains, quantification of fluorescence intensity for these experiments were performed on a standardized region of interest (ROI) capturing the nerve ring but excluding the intestine. Fluorescence intensities at t=24hrs and t=48hrs were normalized to the average posterior pharyngeal bulb diameter of the day one adult cohort imaged at t=0hrs to account for neuronal expansion with nematode growth. A normalization factor for each animal was calculated by dividing the posterior pharyngeal bulb diameter of each worm by the average posterior pharyngeal bulb diameter from the t=0hr cohort, measured using ImageJ. The fluorescence intensity of each sample was divided by this normalization factor to produce the normalized fluorescence intensity.

Statistical analyses

All statistical analyses were performed using GraphPad Prism statistical software (GraphPad Software, Inc., La Jolla, CA, USA). Statistical significance was determined using one-way analysis of variance (ANOVA) with Tukey's multiple-comparison test, one-tailed paired *t*-test, or unpaired two-tailed *t*-test with Welch's correction (*$P < 0.05$, **$P < 0.01$, ***$P < 0.001$, **** $P < 0.0001$). The average values reported are the means, with error bars representing standard error of the mean (SEM).

Results

Multicopy Dendra2::tau *C. elegans* exhibit a range of disease phenotypes

We generated five independent pan-neuronal Dendra2::tau expressing transgenic (Tg) *C. elegans* strains using genomically integrated multicopy arrays (Tg M1-M5) under control of the pan-neuronal *snb-1* promoter (Fig 1A). Dendra2::tau Tg animals were characterized for their tau protein level, behavior, and Dendra2 fluorescence. Dendra2::tau protein expression and behavioral deficits were compared to previously published untagged Tau (high) and Tau (low)

strains (Kraemer *et al.*, 2003; Benbow *et al.*, 2020), which both express wild-type human tau under the pan-neuronal *aex-3* promoter. The five Dendra2::tau transgenic strains exhibited a broad range of tau protein expression (Fig 1B, C) correlating with motility impairment (Fig 1D, F), with higher tau levels corresponding to greater motility deficits in a manner consistent with an exponential decay relationship (Fig 1E, G). To better differentiate the level of motility impairment between Tau (high), Tg M1, and Tg M2, we performed a radial assay that shows Tg M1 and Tg M2 disperse significantly less over a 24hr period compared to Tau (high) (Fig 1F), as would be expected from the higher burden of tau in these strains. Therefore, we attribute the lack of a significant difference between Tg M1, Tg M2, and Tau (high) in the swimming assay to a floor effect in the motor program measured by this assay. Confocal microscopy confirmed that the Dendra2 construct was indeed expressed in a neuronal pattern (Fig 1H). By qualitative observation, the Dendra2 fluorescence intensity of the multicopy strains correspond to their relative tau protein levels. In summary, we have generated a collection of Dendra2::tau strains with a broad range of pan-neuronal tau expression levels driving increasingly severe behavioral phenotypes.

Single-copy Dendra2::tau *C. elegans* display wild-type phenotype

Many *C. elegans* models of neurodegenerative disease utilize extrachromosomal arrays or integrated transgenes expressing a disease-related protein. To address concerns raised about the potential differences between multicopy versus single-copy transgenic strategies, we generated *C. elegans* strains with a single copy of genomically integrated Dendra2::tau using recombinase-mediated cassette exchange (Fig 2A) (Nonet, 2020). When compared to untagged tau strains [Tau (high) and Tau (low)] and the lowest expression multicopy strain Tg M5, all four of the single-copy Dendra2::tau strains exhibit very low levels of tau protein (Fig 2B, C), and perform similarly to wild-type N2 in the swimming assay (Fig 2D). The low level of tau is reflected in a very low fluorescence signal of Dendra2::tau detected by confocal microscopy, as compared to the lowest expressing multicopy Dendra2::tau Tg M5 strain (Fig 2E).

To determine the usefulness of this model, we co-expressed single-copy Dendra2::tau with the known tau enhancer, wild-type human transactive response DNA-binding protein (TDP-43) (Latimer *et al.*, 2022). Dendra2::tau fluorescence quantitated from confocal microscopy images revealed increased fluorescence intensity when single-copy Dendra2::tau was co-expressed with TDP-43 (Fig S2 A, B). We also show that TDP-43 expression exacerbated motor impairment of single-copy Dendra2::tau animals at day one and day five of adulthood (Fig

S2 C, D), demonstrating the utility of the single-copy Dendra2::tau model in detecting tauopathy phenotype exacerbation.

Dendra2::tau protein turnover is faster than Dendra2

The monomeric fluorescent protein Dendra2 irreversibly converts from green to red fluorescence upon exposure to 405nm light. Photoconversion of Dendra2::tau facilitates optical pulse-chase experiments by enabling measurement of red fluorescence decay, which represents pulse-labeled tau degradation. Meanwhile, return of green fluorescence indicates synthesis of new tau protein.

Previous studies found that photoconverted Dendra2 is stable and does not decay significantly over 200 minutes in HEK293 cells (Zhang *et al.*, 2007) or over 24 hours in *C. elegans* (Hamer, Matilainen and Holmberg, 2010). On the other hand, Dendra2::2N4R tau red fluorescent signal decays to ~20% of original intensity after 36 hours in zebrafish (Lopez *et al.*, 2017). In contrast, Dendra2 and Dendra2::0N4R tau in mouse brain slice culture exhibited similar half-lives of 2.47 and 2.67 days, respectively (Croft *et al.*, 2021).

We generated control strains expressing the Dendra2 protein by itself under the same pan-neuronal *snb-1* promoter. Dendra2 is at most minimally toxic based on performance in a motility assay (Fig S1). Of the multiple Dendra2 strains generated, the strain with no quantifiable behavioral deficits and lowest Dendra2 fluorescence was chosen for this experiment to avoid toxicity from high Dendra2 transgene expression (Fig S1).

Day one adult Dendra2 and Dendra2::tau Tg M4 strains were photoconverted and serially imaged over 48 hours (Fig 3, Fig S3). Tg M4 was selected for this experiment due to its intermediate level of Dendra2::tau expression compared to other strains and feasibility of imaging with the same optical configuration as the Dendra2 control strain.

Dendra2 and Dendra2::tau green fluorescence decreased upon photoconversion and never returned to initial intensity levels, replicating earlier studies (Hamer, Matilainen and Holmberg, 2010; Bolková and Lanctôt, 2016). We found that photoconverted Dendra2 red fluorescence decreased by 22.9% over 48hrs, while photoconverted Dendra2::tau red fluorescence decreased by 47.7% during the same time, indicating that Dendra2::tau protein turnover rate is higher than that of Dendra2 alone. The relative stability of photoconverted Dendra2 alone recapitulates previous studies (Zhang *et al.*, 2007; Hamer, Matilainen and Holmberg, 2010).

Dendra2::tau protein expression level affects degradation rate

A double transgenic strain, hereby referred to as “double copy,” was generated by crossing two single-copy strains Tg S1 and Tg S3, resulting in greater Dendra2 fluorescence that enabled direct comparison with the low expression multicopy strain Tg M5. To determine whether Dendra2::tau turnover rate changes with expression level of the protein, the double copy and Tg M5 strains were photoconverted and serially imaged over 48hrs. While newly synthesized green Dendra2::tau levels increased over 48hrs in both strains (Fig 4A, C), the turnover of photoconverted red Dendra2::tau differed between strains. The double copy strain failed to exhibit significant turnover of Dendra2::tau over 48hrs, while the Tg M5 strain demonstrated significant degradation of the protein, resulting in a 20.5% decrease over 48hrs (Fig 4B, D).

Our findings indicate that lower Dendra2::tau expression results in less turnover over 48hrs. While the complete lack of turnover in the double copy strain may be surprising, it is possible that the amount of Dendra2::tau in this strain is insufficient stress to activate neuronal protein degradative pathways, resulting in no clearance of the protein.

TDP-43 enhances Dendra2::tau and Dendra2 phenotype but does not alter Dendra2::tau protein turnover

Our group previously showed strong enhancement of tau pathology in untagged wild-type human tau transgenic *C. elegans* by wild-type human TDP-43 (Latimer *et al.*, 2022). The tau strain exhibited a mild disease phenotype alone but a moderate to strong disease phenotype with TDP-43, a phenomenon recapitulated in Dendra2::tau *C. elegans* (Fig 5 A, B, C). We crossed a low expression wild-type human TDP-43 strain (CK1943) with Dendra2::tau Tg M5, which expresses the lowest level of Dendra2::tau amongst the multicopy strains. Tg M5 was chosen for this experiment because higher expression of tau compromises viability in combination with the TDP-43 transgene. Co-expression of TDP-43 with Dendra2::tau increased tau protein accumulation, exacerbated motor deficits, and enhanced fluorescence intensity (Fig 5). Dendra2::tau; TDP-43 animals showed increased fluorescence intensity in the head and nerve cord (Fig 5D, E, F), as well as increased puncta number (Fig 5G) but no change in puncta area in the head (Fig 5H). Nerve cord puncta could not be quantified due to high background signal. These data suggest that TDP-43 drives Dendra2::tau accumulation or impairs its degradation and promotes the aggregation of Dendra2::tau into visible puncta. Furthermore, TDP-43 enhancement of Dendra2::tau was observed in the single-copy Dendra2::tau strain Tg S1 over the course of aging (Fig S1).

Surprisingly, TDP-43 increased fluorescence intensity and puncta number in the head of Dendra2-only animals (Fig 5I, J, K) and decreased motility (Fig 5C), but not to the same extent as for Dendra2::tau. Therefore, we suspect that TDP-43 impairs general proteostasis of Dendra2 as a long-lived protein in the neuron, as it has been shown that TDP-43 perturbs various proteostasis mechanisms (Leibiger *et al.*, no date; Ormeño *et al.*, 2020; de Mena, Lopez-Scarim and Rincon-Limas, 2021; Yin *et al.*, 2021).

To determine whether TDP-43 affects Dendra2::tau protein turnover, we generated a new Dendra2::tau Tg M5; TDP-43 strain using a different low expression wild-type human TDP-43 strain (CK402) with a fluorescent reporter compatible with acquisition of photoconverted red Dendra2::tau. This new Dendra2::tau Tg M5; TDP-43 strain also exhibited behavioral impairment in the swimming assay compared to Tg M5 alone (Fig 6A). Upon photoconversion, the Dendra2::tau Tg M5 and Dendra2::tau Tg M5; TDP-43 strains exhibited a similar proportion of Dendra2::tau turnover (39.6% vs 41.4% decrease, respectively) over 48hrs (Fig 6B, 6C). These results indicate that while TDP-43 increases Dendra2::tau accumulation, it does not impair Dendra2::tau degradation.

Suppressors of tauopathy differentially interact with Dendra2::tau

We crossed known genetic suppressors of tauopathy (*sut* genes) into the moderate expression Dendra2::tau strain Tg M4, which displays a strong behavioral and fluorescent phenotype for detection of genetic suppression. We expected to observe levels of Dendra2::tau suppression similar to previous findings in untagged tau backgrounds (Table 3). However, we found that *sut-2* did not suppress Dendra2::tau phenotypes tested, including fluorescence intensity, motility, or tau protein accumulation (Fig 7B, E, F, G). Interestingly, while *spop-1* suppressed motility defects of Dendra2::tau more strongly than *xbp-1s* (Fig 7E), both *spop-1* and *xbp-1s* suppressed accumulation of Dendra2::tau to similarly low levels (Fig 7G). In summary, not all *sut* genes shown to suppress tauopathy phenotypes driven by untagged tau suppressed tauopathy phenotype in the Dendra2::tau model. Additionally, the degree of suppression of Dendra2::tau fluorescence and motility will not necessarily correspond for a given *sut* gene.

Conclusion

In AD and other tauopathies, neurons must clear pathological tau to maintain neuronal health, and failure to do so results in tau aggregation, neuronal dysfunction, and neurodegeneration. Understanding regulation of tau proteostasis is key to developing treatments that can modulate

tau accumulation and clearance in disease. Investigation of tau proteostasis mechanisms would benefit from the capacity to visualize tau *in vivo* in a genetically tractable model organism in which mammalian proteostasis pathways are conserved.

We present Dendra2::tau transgenic *C. elegans* as a useful tool for modeling tau proteostasis. We found that, congruent with untagged tau models, Dendra2-tagged tau burden correlated positively with phenotype severity in multicopy Dendra2::tau Tg strains. Meanwhile, single-copy Dendra2::tau Tg strains lack obvious disease-related phenotypes due to low tau levels. The lack of a distinct disease phenotype in this single-copy model indicates the usefulness of multicopy arrays in modeling disease in *C. elegans*. Given the known high levels of neuronal tau occurring *in vivo* in disease states and the low level tau expressed from single-copy transgenic strains, the single-copy strategy seems poorly suited for modeling tauopathy but could be suitable for identifying genetic enhancers and pathways contributing to tau proteostasis.

Investigating effects of known tau suppressors on the Dendra2::tau model revealed interesting results. The *sut* genes *spop-1* and *xbp-1s* suppressed Dendra2::tau fluorescence, accumulation, and motility similarly to previously published effects on untagged tau, while *sut-2* failed to suppress at all. These discrepancies may be due to disrupted protein-protein interactions and could be used to help elucidate the mechanism by which each *sut* gene suppresses tau phenotype. A known enhancer of tauopathy, wild-type human TDP-43, enhanced the fluorescence and behavioral phenotype of a low expression Dendra2::tau strain. Interestingly, wild-type human TDP-43 produced a similar effect in a Dendra2-only control strain, suggesting that TDP-43 disrupts general proteostasis in neurons (Leibiger *et al.*, no date; Xia *et al.*, 2016; Lee *et al.*, 2020; Ormeño *et al.*, 2020; Yin *et al.*, 2021; Keating *et al.*, 2022).

In addition to the abundance and localization of the tagged protein, Dendra2 can be used to determine the turnover rate of the protein of interest by optical pulse labeling. Photoconversion of Dendra2 and Dendra2::tau animals showed Dendra2::tau turnover to be faster than that of Dendra2 alone. Our results support previous publications, which show that Dendra2 is as stable if not more stable than Dendra2::tau. Small discrepancies between our results and previously published reports can be attributable to differences in expression level, transgene promoter, tau isoform, or model organism. Photoconversion of the double copy Dendra2::tau strain compared to the lowest expression multicopy Tg M5 strain showed that less Dendra2::tau expression resulted in less turnover of the protein, which may be due to insufficient activation of proteostatic pathways by the low level of Dendra2::tau expression in the double copy. Interestingly, TDP-43 did not change the rate of Dendra2::tau degradation.

Although we had expected TDP-43 to impair Dendra2::tau turnover since TDP-43 dysregulates proteostatic pathways (Leibiger *et al.*, no date; Ormeño *et al.*, 2020; Yin *et al.*, 2021), our results suggest that TDP-43 does not stabilize Dendra2::tau but instead promotes its accumulation possibly through enhanced protein synthesis to enhance tauopathy phenotype. It is also possible that the higher expression of Dendra2::tau protein in the Dendra2::tau Tg M5; TDP-43 strain more strongly activated neuronal proteostatic pathways such as ER stress signaling (Walker *et al.*, 2013; de Mena, Lopez-Scarim and Rincon-Limas, 2021) to clear Dendra2::tau, compensating for proteostasis impairment by TDP-43. Future investigation will determine which proteostasis pathways – UPS, ALP, or UPR – participate in TDP-43 enhancement of Dendra2::tau alone.

C. elegans is an ideal organism for *in vivo* visualization of fluorescently tagged proteins due to its optical transparency. Recently, Aquino Nunez *et al.* presented a GFP-tagged tau *C. elegans* model which differs substantially from our Dendra2::tau model in that it 1) is expressed under the *rgef-1* promoter, 2) fuses GFP to the C terminus of tau, 3) lacks a disease phenotype without aging, and 4) lacks visible tau aggregates (Nunez *et al.*, 2022). Since the initial description of Dendra2 as a photoconvertible protein in 2006 (Gurskaya *et al.*, 2006), Guha *et al.* is the only other group to utilize Dendra2::tau as a probe for studying tau function and pathogenesis in *C. elegans* (Guha *et al.*, 2020). In contrast to our multi- and single-copy pan-neuronal snb-1::Dendra2::1N4R WT tau models, Guha *et al.* employed a single copy of mec-7::Dendra2::0N4R tau with phospho-mimetic, phospho-ablative, or acetylation mimetic mutations. In this mechanosensory model, Dendra2 expressed by itself exhibits greater fluorescence compared to Dendra2::tau, in agreement with our pan-neuronal model. Our Dendra2 strain may have integrated a higher copy number of the Dendra2 construct compared to the Dendra2::tau strains because Dendra2 is putatively less toxic than tau, and this higher copy number could be driving increased Dendra2 expression. However, Guha *et al.* used a single-copy model and still observed a similar discrepancy in fluorescence between Dendra2 and Dendra2::tau, suggesting that the fusion of tau to Dendra2 may interfere with fluorophore maturation or excitation. Interestingly, Guha *et al.* do not take advantage of the photoconvertible utility of Dendra2. It is also possible that they encountered the limitations that we describe below.

There are several previously noted limitations to using Dendra2 to visualize and monitor a protein of interest (POI) (Pigazzini and Kirstein, 2020). It is most often used as an exogenous overexpression construct, such that the POI and Dendra2 are not expressed at normal physiological levels in the organism. Further, the rate of Dendra2 degradation could affect the

degradation rate of the fused POI. Dendra2 has been shown to be highly stable, and in our model that could mean enhanced stability for tau due to Dendra2 fusion, or vice versa. In contrast, Dendra2 cannot be used to monitor proteins with fast turnover because of the time required for photoconversion and fluorophore maturation. The optimal wavelength for photoconversion is 405nm, which happens to be toxic to *C. elegans*; while Dendra2 can also be photoconverted by a 488nm wavelength light, this means that intensive imaging in the 488nm channel can also drive photoconversion (Bolková and Lanctôt, 2016). Indeed, we observed this phenomenon when attempting fluorescence recovery after photobleaching (FRAP), which measures diffusion of Dendra2::tau into a photobleached region of interest. This suggests that other more stable non-photoconvertible eGFP derivatives may be more suitable fusion partners for tau FRAP experiments than Dendra2.

Dendra2 also posed several challenges that complicated its use as a photoconvertible protein for optical pulse labeling experiments. First, it was impossible to achieve 100% efficiency of photoconversion. Li *et al*. reported a photoconversion efficiency of >60% (Li *et al.*, 2011), and, to the best of our knowledge, no group that has explicitly reported their data has demonstrated anywhere near 100% efficiency. While the lack of complete photoconversion does not preclude optical pulse labeling experiments, the Dendra2 protein also exhibited incomplete turnover over a measurable time frame of 48hrs. Dendra2 by itself is extremely stable after photoconversion for 200min (Zhang *et al.*, 2007) and 24hrs (Hamer, Matilainen and Holmberg, 2010), making the Dendra2-only model a control with limited utility when trying to assess the stability of a Dendra2-fused protein. Furthermore, no Dendra2-fused proteins reported thus far have exhibited 100% turnover in the measured time frame. For instance, Hamer *et al.* show ~30% (12hrs) and ~50% (24hrs) degradation of whole-organism Dendra2 red fluorescence in their UbG76V-Dendra2 *C. elegans* model (Hamer, Matilainen and Holmberg, 2010). Pigazzini *et al.* also showed lack of complete turnover of HTT-D2 in a single *C. elegans* neuron at 2hrs and 24hrs post-photoconversion (Pigazzini and Kirstein, 2020). Lopez *et al.* demonstrated up to 80% reduction of Dendra2::tau and Dendra2-α-SYN in a zebrafish neuron 48hrs post photoconversion (Lopez *et al.*, 2022). Specifically, Croft *et al.* showed that Dendra2 and Dendra2::tau half-life are on the order of days in brain slice cultures (Croft *et al.*, 2021).

Overall, we have shown that the Dendra2::tau model allows immediate visualization of tau localization and abundance. We have developed a suite of Dendra2::tau strains with varying degrees of disease severity suitable for either detection of tauopathy suppression or enhancement. By photoconverting Dendra2, we demonstrated faster turnover of Dendra2 fused to tau compared to Dendra2 alone, and determined the effect of Dendra2::tau expression level

and TDP-43 on Dendra2::tau turnover. This model could expedite the screening process for genetic modifiers of tau accumulation and turnover rate. The Dendra2::tau model allows faster and easier investigation of tau proteostasis and potential identification of pathways that ameliorate tau accumulation and/or promote clearance, which could provide novel molecular targets for treatment of tauopathy.

Acknowledgements

We thank Ashley Sciocchetti, Brandon Henderson, Asia Beale, Jade Stair, and Lisa Chang for outstanding technical assistance. We thank WormBase for model organism information and resources. Strains were provided by the Caenorhabditis Genetics Center, which is funded by National Institute of Health's Office of Research Infrastructure Programs (P40 OD010440), and the Reverse Genetics Core Facility at the Oklahoma Medical Research Foundation and University of British Columbia, which are part of the international *C. elegans* Gene Knockout Consortium. Figures were created with BioRender.com. This material is the result of work supported with resources and the use of facilities at the VA Puget Sound Health Care System.

Funding

This work was supported by grants from the Department of Veterans Affairs [IK6BX006467 to B.K., I01BX004044 to N.L., and a VA PSHCS Director's fellowship to MH], National Institutes of Health [RF1AG055474 & R01NS064131 to B.K and R01AG066729 to N.L.], and the BrightFocus Foundation [A2022041 to N.L.].

References

Abisambra, J.F. *et al.* (2013) 'Tau accumulation activates the unfolded protein response by impairing endoplasmic reticulum-associated degradation', *The Journal of neuroscience : the official journal of the Society for Neuroscience*, 33(22), pp. 9498–9507. Available at: https://doi.org/10.1523/JNEUROSCI.5397-12.2013.

Benbow, S.J. *et al.* (2020) 'Synergistic toxicity between tau and amyloid drives neuronal dysfunction and neurodegeneration in transgenic C. elegans.', *Human molecular genetics*, 29(3), pp. 495–505. Available at: https://doi.org/10.1093/hmg/ddz319.

Bolková, J. and Lanctôt, C. (2016) ‘Live imaging reveals spatial separation of parental chromatin until the four-cell stage in Caenorhabditis elegans embryos’, *International Journal of Developmental Biology*, 60(1-2–3), pp. 5–12. Available at: https://doi.org/10.1387/IJDB.150222CL.

Brenner, S. (1974) ‘The genetics of Caenorhabditis elegans’, *Genetics*, 77(1), pp. 71–94. Available at: https://doi.org/10.1093/GENETICS/77.1.71.

Bruch, J. *et al.* (2017) ‘PERK activation mitigates tau pathology in vitro and in vivo’, *EMBO Molecular Medicine*, 9(3), p. 371. Available at: https://doi.org/10.15252/EMMM.201606664.

Caballero, B. *et al.* (2021) ‘Acetylated tau inhibits chaperone-mediated autophagy and promotes tau pathology propagation in mice’, *Nature communications*, 12(1). Available at: https://doi.org/10.1038/S41467-021-22501-9.

Chen, X. *et al.* (2020) ‘Promoting tau secretion and propagation by hyperactive p300/CBP via autophagy-lysosomal pathway in tauopathy’, *Molecular neurodegeneration*, 15(1). Available at: https://doi.org/10.1186/S13024-019-0354-0.

Chudakov, D.M., Lukyanov, S. and Lukyanov, K.A. (2007) ‘Using photoactivatable fluorescent protein Dendra2 to track protein movement’, *BioTechniques*, 42(5), pp. 553–565. Available at: https://doi.org/10.2144/000112470.

Croft, C.L. *et al.* (2021) ‘Photodynamic studies reveal rapid formation and appreciable turnover of tau inclusions’, *Acta Neuropathologica*, 141(3), p. 359. Available at: https://doi.org/10.1007/S00401-021-02264-9.

Currey, H.N. and Liachko, N.F. (2021) ‘Evaluation of Motor Impairment in C. elegans Models of Amyotrophic Lateral Sclerosis’, *Journal of visualized experiments : JoVE*, 2021(175). Available at: https://doi.org/10.3791/62699.

Dickey, C.A. *et al.* (2006) ‘Deletion of the ubiquitin ligase CHIP leads to the accumulation, but not the aggregation, of both endogenous phospho- and caspase-3-cleaved tau species’, *The Journal of neuroscience : the official journal of the Society for Neuroscience*, 26(26), pp. 6985–6996. Available at: https://doi.org/10.1523/JNEUROSCI.0746-06.2006.

Dolan, P.J. and Johnson, G.V.W. (2010) ‘A caspase cleaved form of tau is preferentially degraded through the autophagy pathway’, *The Journal of biological chemistry*, 285(29), pp. 21978–21987. Available at: https://doi.org/10.1074/JBC.M110.110940.

Eck, R.J. *et al.* (2023) ‘SPOP loss of function protects against tauopathy’, *Proceedings of the National Academy of Sciences of the United States of America*, 120(1), p. e2207250120. Available at: https://doi.org/10.1073/PNAS.2207250120/SUPPL_FILE/PNAS.2207250120.SAPP.PDF.

Feng, Q. *et al.* (2020) 'MAPT/Tau accumulation represses autophagy flux by disrupting IST1-regulated ESCRT-III complex formation: a vicious cycle in Alzheimer neurodegeneration', *Autophagy*, 16(4), pp. 641–658. Available at: https://doi.org/10.1080/15548627.2019.1633862.
Gallo, D., Ruiz, A. and Sánchez-Juan, P. (2022) 'Genetic Architecture of Primary Tauopathies', *Neuroscience* [Preprint]. Available at: https://doi.org/10.1016/J.NEUROSCIENCE.2022.05.022.
Ginsberg, S.D. *et al.* (1997) 'Sequestration of RNA in Alzheimer's disease neurofibrillary tangles and senile plaques', *Annals of neurology*, 41(2), pp. 200–209. Available at: https://doi.org/10.1002/ANA.410410211.
Guha, S. *et al.* (2020) 'Tauopathy-associated tau modifications selectively impact neurodegeneration and mitophagy in a novel C. elegans single-copy transgenic model', 15(1), p. 65. Available at: https://doi.org/10.1186/S13024-020-00410-7.
Gurskaya, N.G. *et al.* (2006) 'Engineering of a monomeric green-to-red photoactivatable fluorescent protein induced by blue light', *Nature Biotechnology 2006 24:4*, 24(4), pp. 461–465. Available at: https://doi.org/10.1038/nbt1191.
Guthrie, C.R., Schellenberg, G.D. and Kraemer, B.C. (2009) 'SUT-2 potentiates tau-induced neurotoxicity in Caenorhabditis elegans', *Human Molecular Genetics*, 18(10), p. 1825. Available at: https://doi.org/10.1093/HMG/DDP099.
Hamano, T. *et al.* (2021) 'Autophagy and Tau Protein', *International Journal of Molecular Sciences*, 22(14). Available at: https://doi.org/10.3390/IJMS22147475.
Hamer, G., Matilainen, O. and Holmberg, C.I. (2010) 'A photoconvertible reporter of the ubiquitin-proteasome system in vivo', *Nature Methods 2010 7:6*, 7(6), pp. 473–478. Available at: https://doi.org/10.1038/nmeth.1460.
Hetz, C. (2021) 'Adapting the proteostasis capacity to sustain brain healthspan', *Cell*, 184(6), pp. 1545–1560. Available at: https://doi.org/10.1016/J.CELL.2021.02.007.
Ho, Y.S. *et al.* (2012) 'Endoplasmic reticulum stress induces tau pathology and forms a vicious cycle: implication in Alzheimer's disease pathogenesis', *Journal of Alzheimer's disease : JAD*, 28(4), pp. 839–854. Available at: https://doi.org/10.3233/JAD-2011-111037.
Hoozemans, J.J.M. *et al.* (2005) 'The unfolded protein response is activated in Alzheimer's disease', *Acta neuropathologica*, 110(2), pp. 165–172. Available at: https://doi.org/10.1007/S00401-005-1038-0.
Hoozemans, J.J.M. *et al.* (2009) 'The unfolded protein response is activated in pretangle neurons in Alzheimer's disease hippocampus', *The American journal of pathology*, 174(4), pp. 1241–1251. Available at: https://doi.org/10.2353/AJPATH.2009.080814.

Ittner, A. and Ittner, L.M. (2018) 'Dendritic Tau in Alzheimer's Disease', *Neuron*, 99(1), pp. 13–27. Available at: https://doi.org/10.1016/J.NEURON.2018.06.003.
Keating, S.S. *et al.* (2022) 'TDP-43 pathology: From noxious assembly to therapeutic removal', *Progress in Neurobiology*, 211, p. 102229. Available at: https://doi.org/10.1016/J.PNEUROBIO.2022.102229.
Kennedy, B.K. *et al.* (2014) 'Geroscience: linking aging to chronic disease', *Cell*, 159(4), pp. 709–713. Available at: https://doi.org/10.1016/J.CELL.2014.10.039.
Kent, S.A., Spires-Jones, T.L. and Durrant, C.S. (2020) 'The physiological roles of tau and Aβ: implications for Alzheimer's disease pathology and therapeutics', *Acta neuropathologica*, 140(4), pp. 417–447. Available at: https://doi.org/10.1007/S00401-020-02196-W.
Kim, J.H. *et al.* (2021) 'CHIP-mediated hyperubiquitylation of tau promotes its self-assembly into the insoluble tau filaments', *Chemical science*, 12(15), pp. 5599–5610. Available at: https://doi.org/10.1039/D1SC00586C.
Kow, R.L. *et al.* (2018) 'DOPA Decarboxylase Modulates Tau Toxicity', *Biological psychiatry*, 83(5), pp. 438–446. Available at: https://doi.org/10.1016/J.BIOPSYCH.2017.06.007.
Kraemer, B.C. *et al.* (2003) 'Neurodegeneration and defective neurotransmission in a Caenorhabditis elegans model of tauopathy', *Proceedings of the National Academy of Sciences of the United States of America*, 100(17), pp. 9980–9985. Available at: https://doi.org/10.1073/PNAS.1533448100.
Latimer, C.S. *et al.* (2022) 'TDP-43 promotes tau accumulation and selective neurotoxicity in bigenic Caenorhabditis elegans', *Disease Models & Mechanisms*, 15(4). Available at: https://doi.org/10.1242/DMM.049323.
Lee, Shinrye *et al.* (2020) 'PTK2/FAK regulates UPS impairment via SQSTM1/p62 phosphorylation in TARDBP/TDP-43 proteinopathies', *Autophagy*, 16(8), pp. 1396–1412. Available at: https://doi.org/10.1080/15548627.2019.1686729.
Leibiger, C. *et al.* (no date) 'TDP-43 controls lysosomal pathways thereby determining its own clearance and cytotoxicity'. Available at: https://doi.org/10.1093/hmg/ddy066.
Lester, E. *et al.* (2021) 'Tau aggregates are RNA-protein assemblies that mislocalize multiple nuclear speckle components', *Neuron*, 109(10), pp. 1675-1691.e9. Available at: https://doi.org/10.1016/J.NEURON.2021.03.026.
Li, X. *et al.* (2011) 'Novel diffusion barrier for axonal retention of Tau in neurons and its failure in neurodegeneration', *The EMBO Journal*, 30(23), p. 4825. Available at: https://doi.org/10.1038/EMBOJ.2011.376.

Loewen, C.A. and Feany, M.B. (2010) 'The Unfolded Protein Response Protects from Tau Neurotoxicity In Vivo', *PLoS ONE*, 5(9), p. 13084. Available at: https://doi.org/10.1371/JOURNAL.PONE.0013084.

Lopez, A. *et al.* (2017) 'A152T tau allele causes neurodegeneration that can be ameliorated in a zebrafish model by autophagy induction', *Brain*, 140(4), p. 1128. Available at: https://doi.org/10.1093/BRAIN/AWX005.

Lopez, A. *et al.* (2022) 'A New Zebrafish Model to Measure Neuronal α-Synuclein Clearance In Vivo', *Genes*, 13(5). Available at: https://doi.org/10.3390/GENES13050868.

López-Otín, C. *et al.* (2013) 'The hallmarks of aging', *Cell*, 153(6), p. 1194. Available at: https://doi.org/10.1016/J.CELL.2013.05.039.

Markaki, M. and Tavernarakis, N. (2010) 'Modeling human diseases in Caenorhabditis elegans', *Biotechnology Journal*, 5(12), pp. 1261–1276. Available at: https://doi.org/10.1002/BIOT.201000183.

de Mena, L., Lopez-Scarim, J. and Rincon-Limas, D.E. (2021) 'TDP-43 and ER Stress in Neurodegeneration: Friends or Foes?', *Frontiers in molecular neuroscience*, 14. Available at: https://doi.org/10.3389/FNMOL.2021.772226.

Mori, H., Kondo, J. and Ihara, Y. (1987) 'Ubiquitin Is a Component of Paired Helical Filaments in Alzheimer's Disease', *Science*, 235(4796), pp. 1641–1644. Available at: https://doi.org/10.1126/SCIENCE.3029875.

Naseri, N.N. *et al.* (2019) 'The complexity of tau in Alzheimer's disease', *Neuroscience letters*, 705, p. 183. Available at: https://doi.org/10.1016/J.NEULET.2019.04.022.

Nelson, P.T. *et al.* (2012) 'Correlation of Alzheimer disease neuropathologic changes with cognitive status: a review of the literature', *Journal of neuropathology and experimental neurology*, 71(5), pp. 362–381. Available at: https://doi.org/10.1097/NEN.0B013E31825018F7.

Nijholt, D.A.T. *et al.* (2012) 'The unfolded protein response is associated with early tau pathology in the hippocampus of tauopathies', *The Journal of pathology*, 226(5), pp. 693–702. Available at: https://doi.org/10.1002/PATH.3969.

Nonet, M.L. (2020) 'Efficient Transgenesis in Caenorhabditis elegans Using Flp Recombinase-Mediated Cassette Exchange', *Genetics*, 215(4), p. 903. Available at: https://doi.org/10.1534/GENETICS.120.303388.

Nunez, W.A. *et al.* (2022) 'Age-dependent accumulation of tau aggregation in Caenorhabditis elegans', *Frontiers in Aging*, 3. Available at: https://doi.org/10.3389/FRAGI.2022.928574.

Ormeño, F. *et al.* (2020) 'Chaperone Mediated Autophagy Degrades TDP-43 Protein and Is Affected by TDP-43 Aggregation', *Frontiers in Molecular Neuroscience*, 13, p. 19. Available at: https://doi.org/10.3389/FNMOL.2020.00019/BIBTEX.

Petrucelli, L. *et al.* (2004) 'CHIP and Hsp70 regulate tau ubiquitination, degradation and aggregation', *Human molecular genetics*, 13(7), pp. 703–714. Available at: https://doi.org/10.1093/HMG/DDH083.

Pigazzini, M.L. and Kirstein, J. (2020) 'In vivo quantification of protein turnover in aging C. Elegans using photoconvertible Dendra2', *Journal of Visualized Experiments*, 2020(160), pp. 1–18. Available at: https://doi.org/10.3791/61196.

PJ, M. *et al.* (2023) 'Tau-RNA complexes inhibit microtubule polymerization and drive disease-relevant conformation change', *Brain : a journal of neurology*, 139(4), pp. 16–17. Available at: https://doi.org/10.1093/BRAIN/AWAD032.

Sahara, N. *et al.* (2005) 'In vivo evidence of CHIP up-regulation attenuating tau aggregation', *Journal of neurochemistry*, 94(5), pp. 1254–1263. Available at: https://doi.org/10.1111/J.1471-4159.2005.03272.X.

Schaeffer, V. *et al.* (2012) 'Stimulation of autophagy reduces neurodegeneration in a mouse model of human tauopathy', *Brain : a journal of neurology*, 135(Pt 7), pp. 2169–2177. Available at: https://doi.org/10.1093/BRAIN/AWS143.

Schneider, C.A., Rasband, W.S. and Eliceiri, K.W. (2012) 'NIH Image to ImageJ: 25 years of Image Analysis', *Nature methods*, 9(7), p. 671. Available at: https://doi.org/10.1038/NMETH.2089.

Shin, Y.H. *et al.* (2021) 'Phenotypic Discovery of Neuroprotective Agents by Regulation of Tau Proteostasis via Stress-Responsive Activation of PERK Signaling', *Angewandte Chemie (International ed. in English)*, 60(4), pp. 1831–1838. Available at: https://doi.org/10.1002/ANIE.202013915.

Strang, K.H., Golde, T.E. and Giasson, B.I. (2019) 'MAPT mutations, tauopathy, and mechanisms of neurodegeneration', *Laboratory investigation; a journal of technical methods and pathology*, 99(7), p. 912. Available at: https://doi.org/10.1038/S41374-019-0197-X.

Stutzbach, L.D. *et al.* (2013) 'The unfolded protein response is activated in disease-affected brain regions in progressive supranuclear palsy and Alzheimer's disease', *Acta Neuropathologica Communications*, 1(1), p. 31. Available at: https://doi.org/10.1186/2051-5960-1-31.

Tang, Z. *et al.* (2015) 'mTor mediates tau localization and secretion: Implication for Alzheimer's disease', *Biochimica et biophysica acta*, 1853(7), pp. 1646–1657. Available at: https://doi.org/10.1016/J.BBAMCR.2015.03.003.

Waldherr, S.M. *et al.* (2019) 'Constitutive XBP-1s-mediated activation of the endoplasmic reticulum unfolded protein response protects against pathological tau', *Nature Communications*, 10(1). Available at: https://doi.org/10.1038/s41467-019-12070-3.

Walker, A.K. *et al.* (2013) 'ALS-associated TDP-43 induces endoplasmic reticulum stress, which drives cytoplasmic TDP-43 accumulation and stress granule formation', *PloS one*, 8(11). Available at: https://doi.org/10.1371/JOURNAL.PONE.0081170.

Wang, W. *et al.* (2021) 'A novel small-molecule PROTAC selectively promotes tau clearance to improve cognitive functions in Alzheimer-like models', *Theranostics*, 11(11), pp. 5279–5295. Available at: https://doi.org/10.7150/THNO.55680.

Wang, Y. *et al.* (2009) 'Tau fragmentation, aggregation and clearance: the dual role of lysosomal processing', *Human molecular genetics*, 18(21), pp. 4153–4170. Available at: https://doi.org/10.1093/HMG/DDP367.

Wang, Y. and Mandelkow, E. (2012) 'Degradation of tau protein by autophagy and proteasomal pathways', *Biochemical Society Transactions*, 40(4), pp. 644–652. Available at: https://doi.org/10.1042/BST20120071.

Wang, Y. and Mandelkow, E. (2016) 'Tau in physiology and pathology', *Nature reviews. Neuroscience*, 17(1), pp. 5–21. Available at: https://doi.org/10.1038/NRN.2015.1.

Weng, F. lin and He, L. (2021) 'Disrupted ubiquitin proteasome system underlying tau accumulation in Alzheimer's disease', *Neurobiology of aging*, 99, pp. 79–85. Available at: https://doi.org/10.1016/J.NEUROBIOLAGING.2020.11.015.

Xia, Q. *et al.* (2016) ' TDP -43 loss of function increases TFEB activity and blocks autophagosome–lysosome fusion ', *The EMBO Journal*, 35(2), pp. 121–142. Available at: https://doi.org/10.15252/EMBJ.201591998.

Yin, P. *et al.* (2021) 'Cytoplasmic TDP-43 impairs the activity of the ubiquitin-proteasome system', *Experimental Neurology*, 345, p. 113833. Available at: https://doi.org/10.1016/J.EXPNEUROL.2021.113833.

Zhang, L. *et al.* (2007) 'Method for real-time monitoring of protein degradation at the single cell level', *BioTechniques*, 42(4), pp. 446–450. Available at: https://doi.org/10.2144/000112453/FORMAT/EPUB.

Zhang, Y. *et al.* (2022) 'Tauopathies: new perspectives and challenges', *Molecular Neurodegeneration*, 17(1), p. 28. Available at: https://doi.org/10.1186/S13024-022-00533-Z.

Figures and Tables

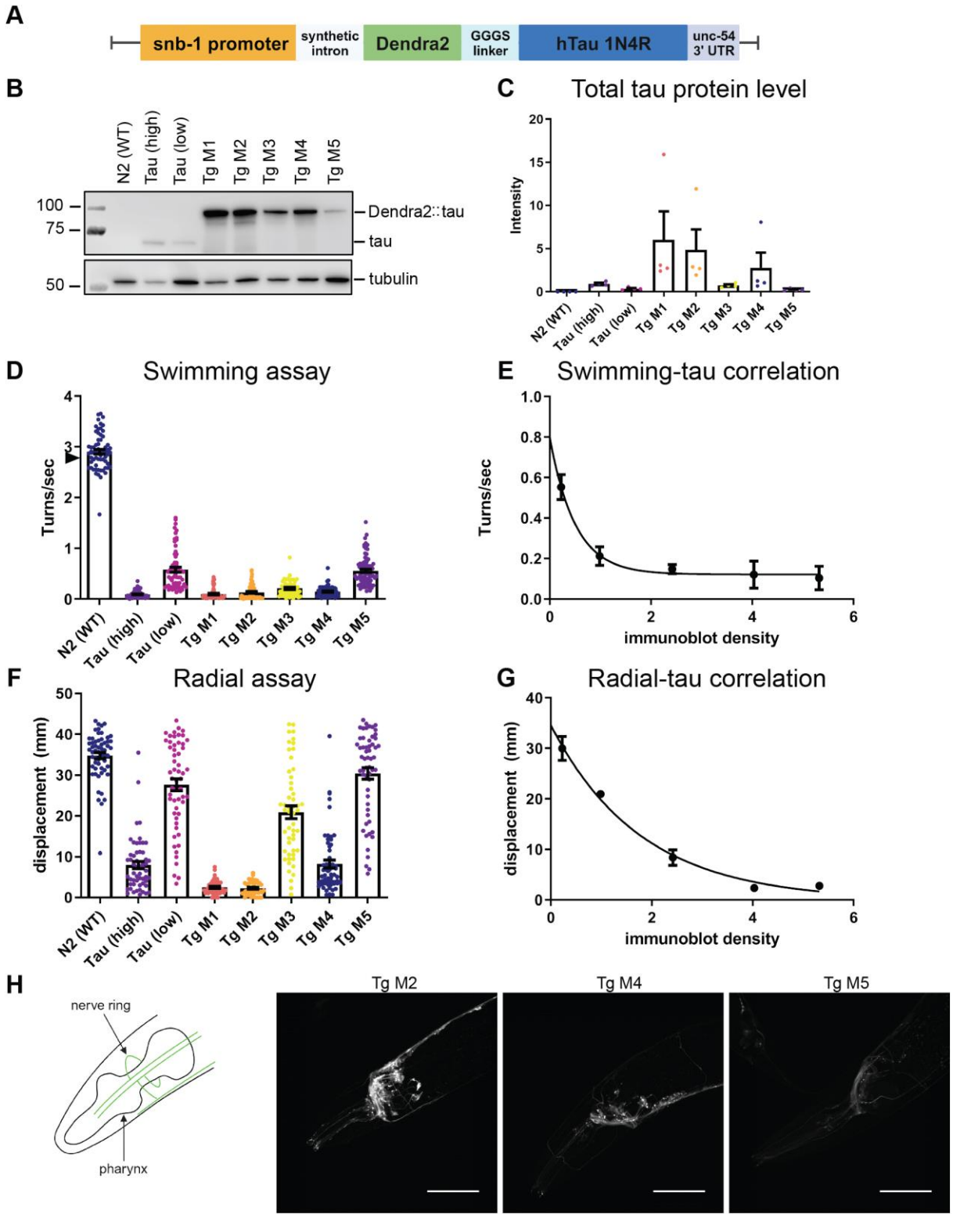

Fig. 1. Multicopy Dendra2::tau level correlates with behavioral phenotype. A DNA construct used for multicopy genomic integration of Dendra2::tau by UV irradiation. Note the Dendra2 construct is driven by the *snb-1* promoter, not the previously published *aex-3* promoter for untagged tau strains. **B** Western blot detecting total tau protein. **C** Western blot quantification of total tau band in untagged and Dendra2-tagged tau strains normalized to tubulin [4 biological replicates; one-way ANOVA with Tukey's multiple comparison test ($p=0.0493$)]. **D** Swimming assay [3 biological replicates; N≥49 animals/strain; one-way ANOVA with Tukey's multiple comparison test ($p<0.0001$)]. Arrowhead indicates average performance of Dendra2-only control strain Tg 2 (Fig S1). **E** Dendra2::tau *C. elegans* swimming behavior correlates with total tau protein level following an exponential decay relationship ($R^2=0.8247$). **F** 24hr radial assay [4 biological replicates; N≥48 animals/strain; one-way ANOVA with Tukey's multiple comparison test ($p<0.0001$)]. **G** Dendra2::tau *C. elegans* radial locomotion correlates with total tau protein level following an exponential decay relationship ($R^2=0.9513$). **H** Representative confocal images of head of three multicopy Dendra2::tau strains. Scale bar: 50µm. Data are mean±SEM.

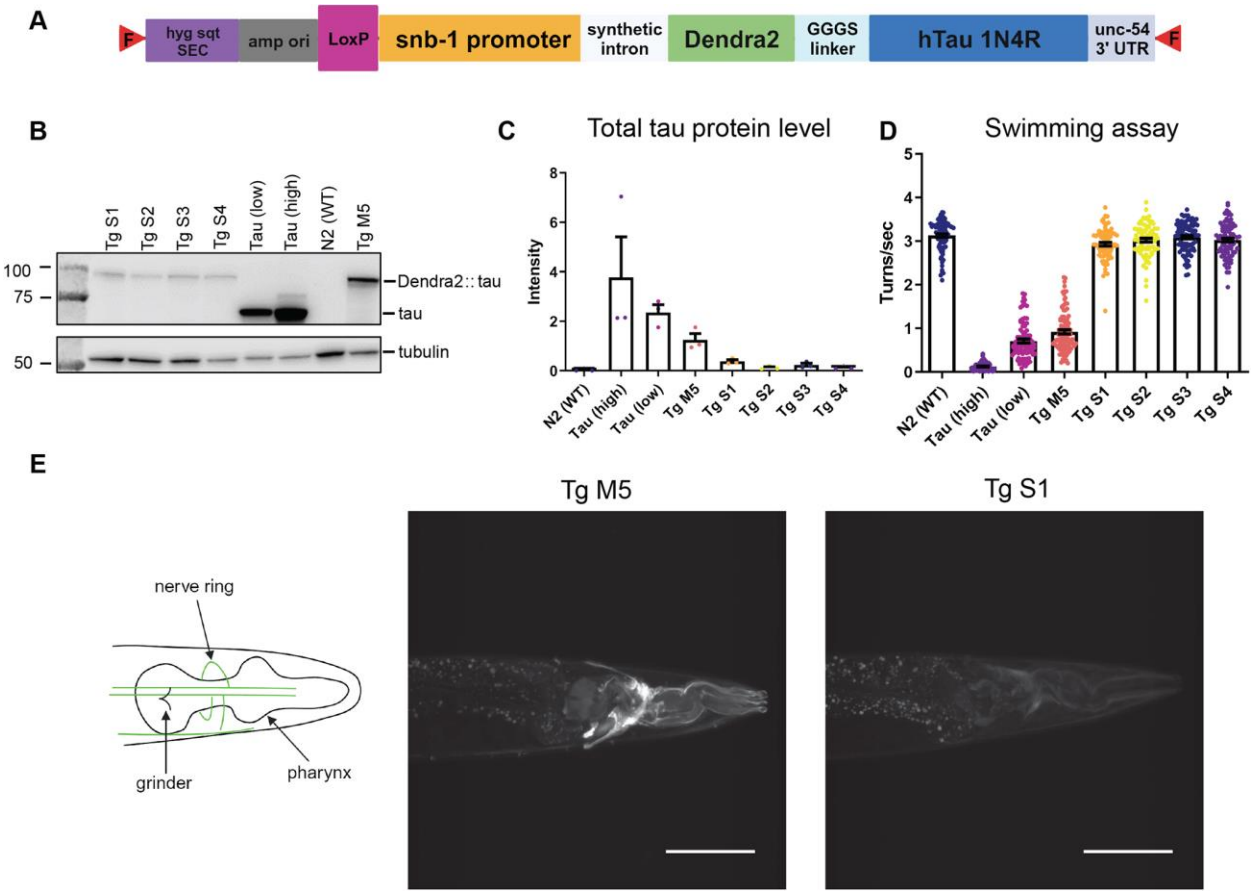

Fig. 2. Single-copy Dendra2::tau does not confer an obvious disease phenotype. **A** DNA construct used for single-copy insertion of Dendra2::tau by dual-component recombinase-mediated cassette exchange in a miniMos landing site (Nonet, 2020). **B** Western blot detecting total tau. **C** Western blot quantification of total tau band in untagged and Dendra2-tagged tau strains normalized to tubulin [3 biological replicates; one-way ANOVA with Tukey's multiple comparison test ($p<0.0001$)]. **D** Swimming assay [4 biological replicates; N≥77 animals/strain; one-way ANOVA with Tukey's multiple comparison test ($p<0.0001$)]. **E** Representative confocal images of the lowest expression Dendra2::tau multicopy strain Tg M5 compared to a representative single-copy Dendra2::tau strain Tg S1. Scale bar: 50µm. Data are mean±SEM. Abbreviations: F: *FRT* site; *hyg sqt* SEC: a self-excising cassette consisting of a promoterless hygromycin resistance gene, the *sqt-1(e1350)* gene, and *cre* recombinase under the control of the *hsp-16.1* promoter; amp: β-lactamase gene; ori: *E. coli* plasmid replication origin.

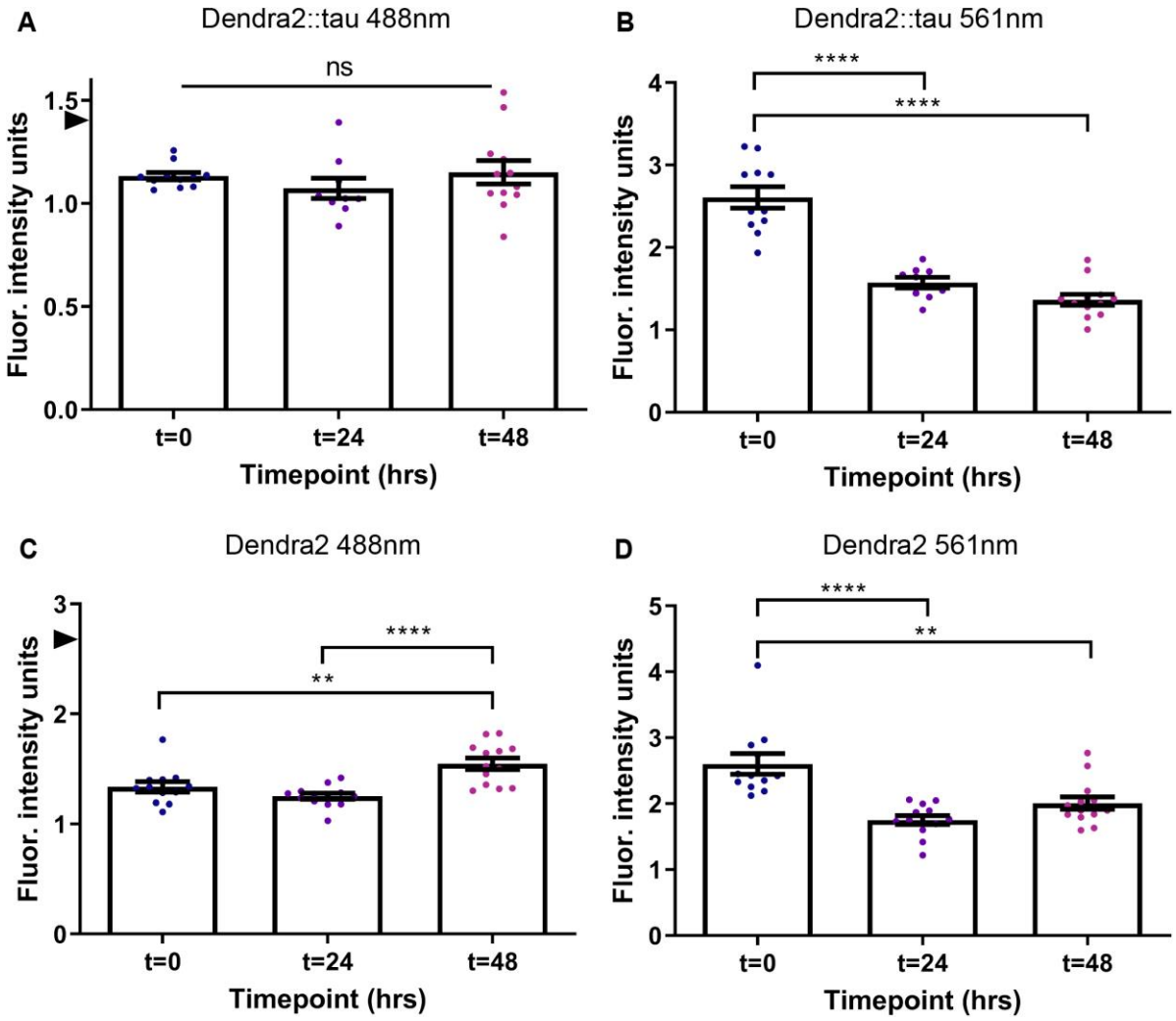

Fig. 3. **Dendra2::tau protein turns over faster than Dendra2.** Mean fluorescence intensity of Dendra2::tau Tg M4 strain head neurons from **A** 488nm [one-way ANOVA with Tukey's multiple comparison test (p=0.4850)] and **B** 561nm wavelength excitation [one-way ANOVA with Tukey's multiple comparison test (p<0.0001)]. Mean fluorescence intensity of Dendra2-only strain head neurons from **C** 488nm [one-way ANOVA w/ Tukey's multiple comparison test (p<0.0001)] and **D** 561nm [one-way ANOVA w/ Tukey's multiple comparison test (p<0.0001)] wavelength excitation. N≥9 animals/strain/timepoint. Arrowhead indicates average fluorescence intensity of nonconverted Dendra2::tau (1.42) and Dendra2 (2.69) signal average in A and C, respectively. 488nm wavelength measures non-photoconverted green Dendra2, while 561nm wavelength measures photoconverted red Dendra2. Representative images in Fig S3. Data are mean±SEM.

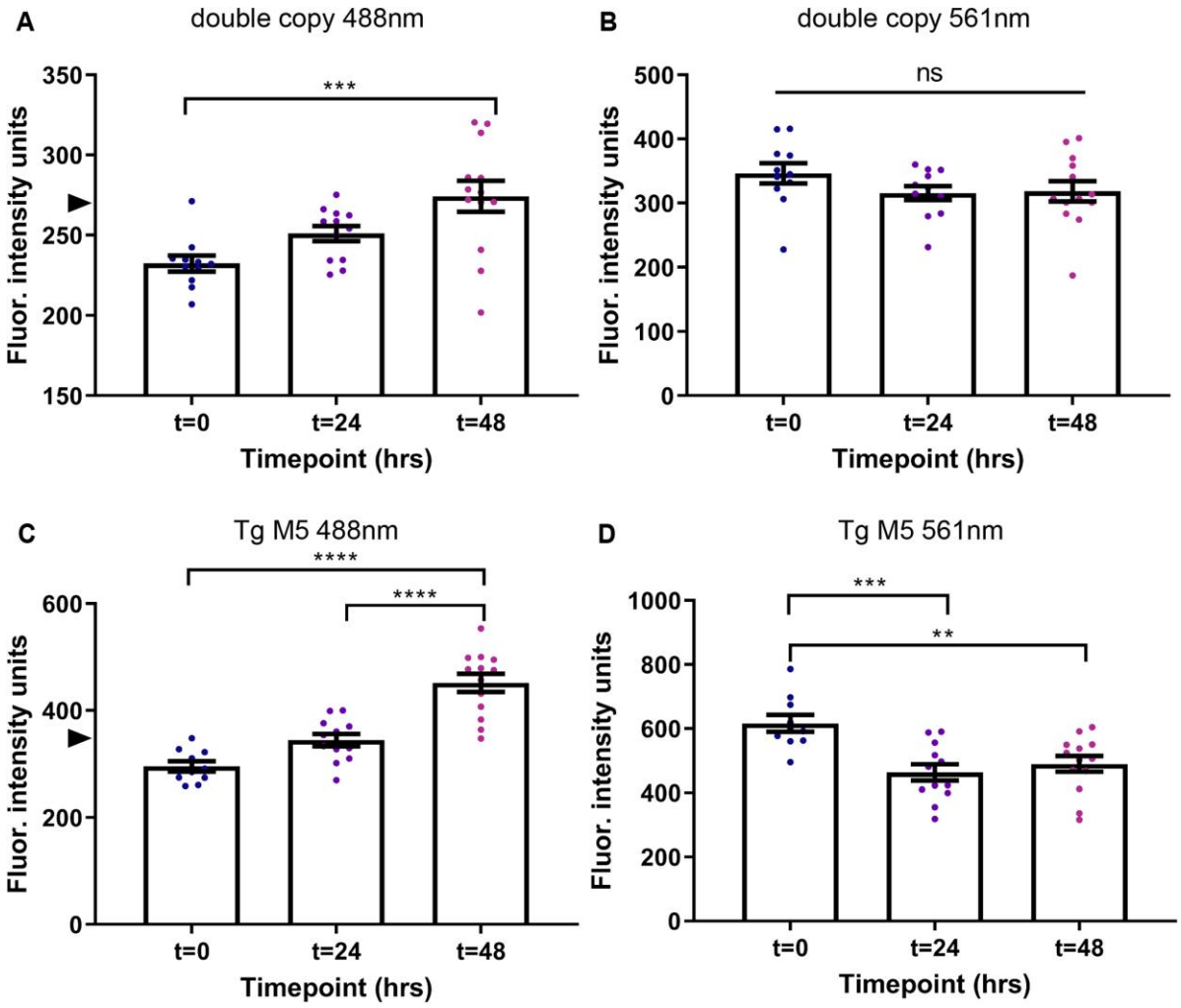

Fig. 4. Dendra2::tau protein turnover depends on expression level. Mean fluorescence intensity of Dendra2::tau double copy strain head neurons from **A** 488nm [one-way ANOVA with Tukey's multiple comparison test (p=0.0009)] and **B** 561nm [one-way ANOVA with Tukey's multiple comparison test (p=0.2799)] wavelength excitation. Mean fluorescence intensity of Dendra2::tau Tg M5 strain head neurons from **C** 488nm [one-way ANOVA with Tukey's multiple comparison test (p<0.0001)] and **D** 561nm [one-way ANOVA with Tukey's multiple comparison test (p=0.0006)] wavelength excitation. N≥10 animals/strain/timepoint. Arrowhead indicates average fluorescence intensity of nonconverted Dendra2::tau in double copy (269.29) and Tg M5 (351.57) in A and C, respectively. 488nm wavelength measures non-photoconverted green Dendra2, while 561nm wavelength measures photoconverted red Dendra2. Representative images in Fig S4. Data are mean±SEM.

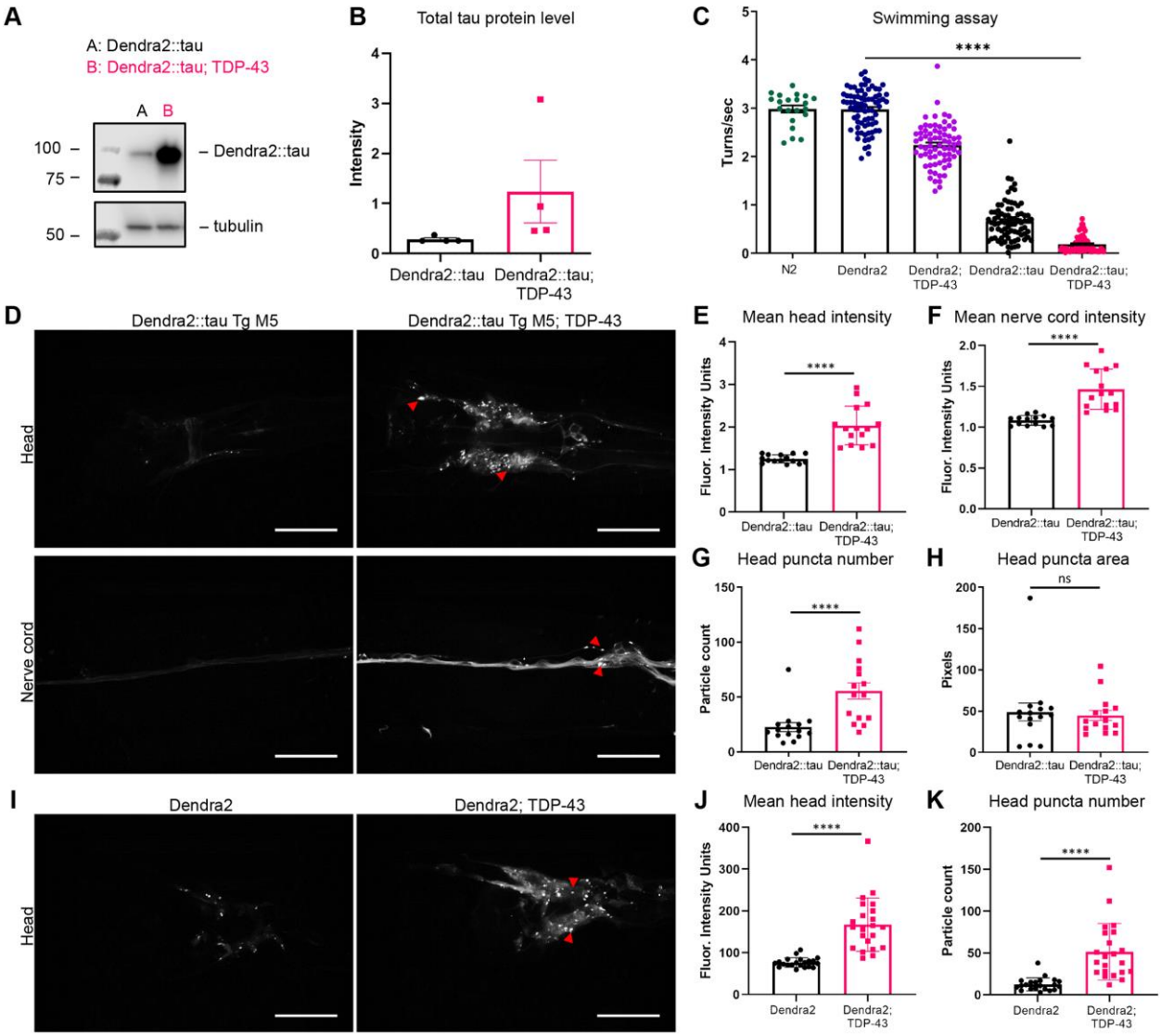

Fig. 5. TDP-43 promotes accumulation of Dendra2::tau and Dendra2 alone. A Representative Western blot detecting total tau in Dendra2::tau Tg M5 strain alone and in TDP-43 (CK1943) background. **B** Quantification of A normalized to tubulin [4 biological replicates; one-tailed paired *t*-test (p=0.1039)]. **C** Swimming assay [4 biological replicates; N≥72 animals/strain; N=21 for N2; one-way ANOVA with Tukey's multiple comparison test (p<0.0001)]. **D** Representative confocal images of head and nerve cord of Dendra2::tau Tg M5 strain alone and in TDP-43 (CK1943) background. Images adjusted with +40% contrast and +40% brightness. **E-F** Quantification of mean

fluorescence intensity in D of head ($p<0.0001$) and nerve cord ($p<0.0001$) ($N\geq14$ animals; unpaired two-tailed *t*-test with Welch's correction). **G-H** Quantification of mean puncta number ($p=0.0008$) and puncta area ($p=0.7357$) in head images in D ($N=15$ animals; unpaired two-tailed *t*-test with Welch's correction). **I** Representative confocal images of head of Dendra2 alone and Dendra2 in TDP-43 (CK1943) background. Images adjusted with +40% contrast and +40% brightness. **J-K** Quantification of mean puncta number ($p<0.0001$) and puncta area ($p<0.0001$) in head images in I ($N\geq21$ animals; unpaired two-tailed *t*-test with Welch's correction). Red arrowheads in representative images indicate puncta. Scale bar: 25μm. Data are mean±SEM.

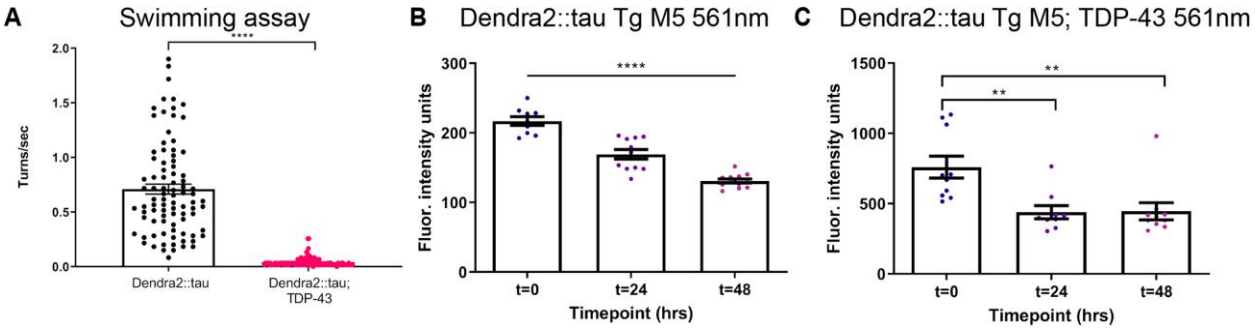

Fig. 6. TDP-43 does not affect Dendra2::tau protein turnover. A Swimming assay of Dendra2::tau Tg M5 alone and in TDP-43 (CK402) background [3 biological replicates; N≥88 animals/strain; unpaired two-tailed *t*-test (p<0.0001)]. **B** Mean fluorescence intensity of Dendra2::tau Tg M5 strain head neurons from 561nm wavelength excitation [one-way ANOVA with Tukey's multiple comparison test (p<0.0001)]. **C** Mean fluorescence intensity of Dendra2::tau Tg M5; TDP-43 (CK402) strain head neurons from 561nm wavelength excitation [one-way ANOVA with Tukey's multiple comparison test (p=0.0017)]. N≥9 animals/strain/timepoint. 561nm wavelength measures photoconverted red Dendra2. Representative images in Fig S5. Data are mean±SEM.

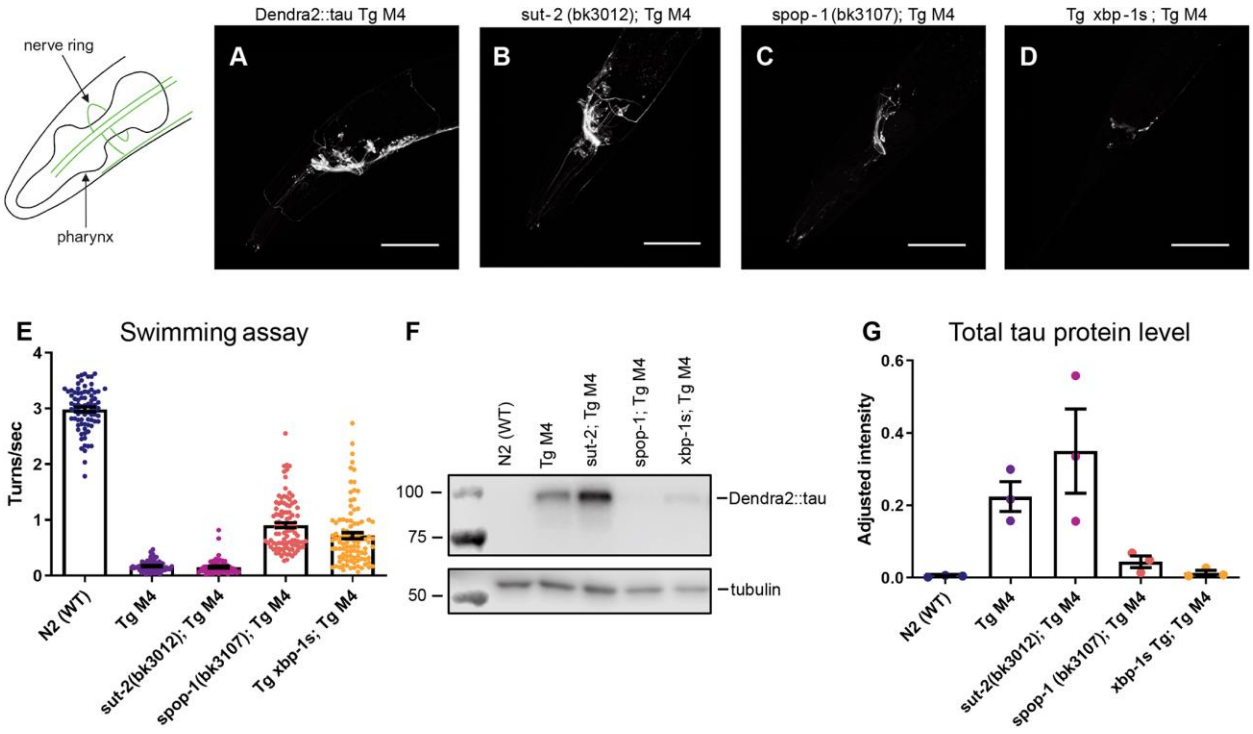

Fig. 7. Differential suppression of Dendra2::tau by known suppressors of tauopathy. A-D Head images of suppressors of tauopathy in Dendra2::tau Tg M4 background. Tail shown for Tg *xbp-1s* due to fluorescent pharyngeal marker. Images adjusted with +40% contrast and +40% brightness. E Swimming assay [4 biological replicates; N≥63 animals; one-way ANOVA with Tukey's multiple comparison test ($p<0.0001$)]. F Western blot of total tau. G Quantification of F normalized to tubulin [3 biological replicates; one-way ANOVA with Tukey's multiple comparison test ($p=0.0045$)]. Scale bar: 50μm. Data are mean±SEM.

Table 1. *C. elegans* strains used in this study.

Strain	Abbreviation	Genotype	Source
N2	N2 (WT)	Bristol, Great Britain wild-type isolate	CGC* (Brenner, 1974)
CK144	Tau (high)	*bkIs144[Paex-3::Tau WT(1N4R); Pmyo-2::GFP]*	(Kraemer *et al.*, 2003)
CK1441	Tau (low)	*bkIs1441[Paex-3::Tau WT(1N4R);Pmyo-2::dsRED]*	(Benbow *et al.*, 2020)
CK2564	Dendra2 Tg 1	*bkIs2564[Psnb-1::Dendra2]*	This study
CK2565	Dendra2 Tg 2	*bkIs2565[Psnb-1::Dendra2]*	This study
CK2566	Dendra2 Tg 3	*bkIs2566[Psnb-1::Dendra2]*	This study
CK2174	Tg M1	*bkIs2174[Psnb-1::Dendra2::hTau WT (1N4R)]*	This study
CK2175	Tg M2	*bkIs2175[Psnb-1::Dendra2::hTau WT (1N4R)]*	This study
CK2176	Tg M3	*bkIs2176[Psnb-1::Dendra2::hTau WT (1N4R)]*	This study
CK2177	Tg M4	*bkIs2177[Psnb-1::Dendra2::hTau WT (1N4R)]*	This study
CK2178	Tg M5	*bkIs2178[Psnb-1::Dendra2::hTau WT (1N4R)]*	This study
CK2351	Tg S1	*bkIs2351[Psnb-1::Dendra2::hTau WT (1N4R)]*	This study
CK2352	Tg S2	*bkIs2352[Psnb-1::Dendra2::hTau WT (1N4R)]*	This study
CK2353	Tg S3	*bkIs2353[Psnb-1::Dendra2::hTau WT (1N4R)]*	This study
CK2354	Tg S4	*bkIs2354[Psnb-1::Dendra2::hTau WT (1N4R)]*	This study
CK2188	*sut-2;* Tg M4	*sut-2(bk3012)*; *bkIs2177[Psnb-1::Dendra2::hTau WT (1N4R)]*	This study
CK2216	*Tg xbp-1s;* Tg M4	*uthIs270[rab-3p::xbp-1s, myo-2p::tdTomato];*	This study

		bkIs2177[Psnb-1::Dendra2::hTau WT (1N4R)]	
CK2546	*spop-1;* Tg M4	*spop-1(bk3107)*; *bkIs2177[Psnb-1::Dendra2::hTau WT (1N4R)]*	This study
CK1943	TDP-43	*bkIs1943[Psnb-1::hTDP-43 WT::K4aptazyme::unc-54 3'UTR+Pmyo-3::mCherry]*	(Latimer *et al.*, 2022)
CK2656	TDP-43; Dendra2::tau Tg M5	*bkIs2178[Psnb-1::Dendra2::hTau WT (1N4R)]; bkIs1943[Psnb-1::hTDP-43 WT::K4aptazyme::unc-54 3'UTR+Pmyo-3::mCherry]*	This study
CK402	TDP-43	*bkIs402[Psnb-1::TDP-43 WT + Pmyo-3::GFP]*	(Currey and Liachko, 2021)

** CGC: Caenorhabditis Genetics Center.*

Table 2. Antibodies used in this study.

Antigen	Host species	Source	Catalog #/clone	Concentration
Tau	Rabbit	Dako	A0024	1:500,000
β-tubulin	Mouse	Developmental Studies Hybridoma Bank	E7	1:5000
Anti-rabbit HRP (secondary)	Goat	Jackson Immuno Research	111-035-144	1:5000
Anti-mouse HRP (secondary)	Goat	Jackson Immuno Research	111-035-146	1:5000

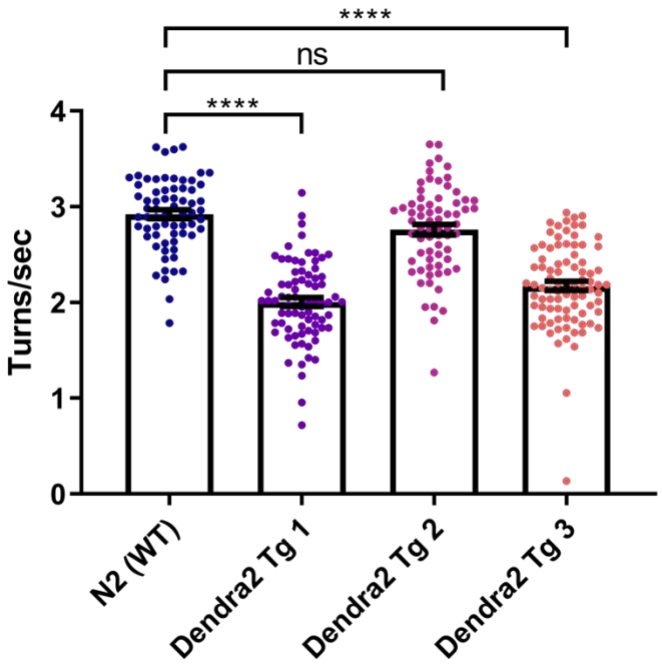

Fig. S1. Dendra2 alone causes minimal neurological impairment measured by swimming assay. [3 biological replicates; N≥67 animals; 1-way ANOVA with Tukey's multiple comparison test ($p<0.0001$)]. Dendra2 Tg 2 strain chosen for experimentation due to no significant difference in swimming performance compared to N2. Error bars: SEM.

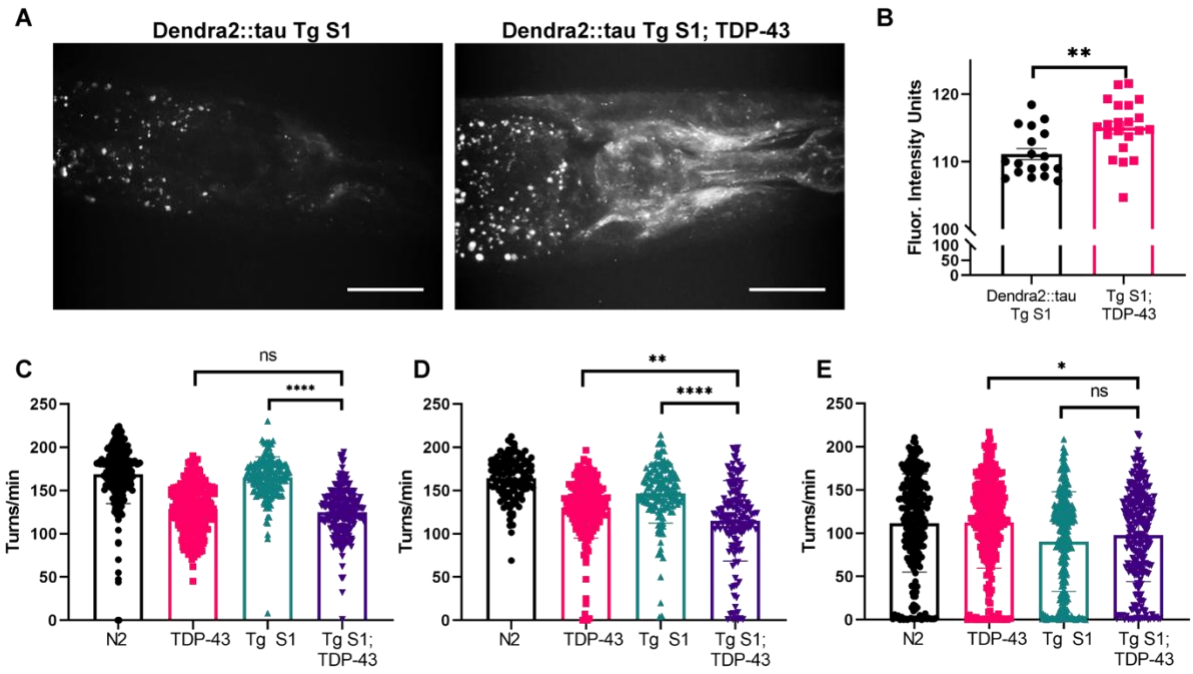

Fig. S2. TDP-43 enhances disease phenotype of single-copy Dendra2::tau *C. elegans*. A Representative images of day one adult single-copy Dendra2::tau Tg S1 with and without wild-type human TDP-43 co-expression. **B** Mean fluorescence intensity of head images from single-copy Dendra2::tau Tg S1 with and without wild-type human TDP-43 co-expression. Swimming assay from **C** day one adults [3 biological replicates; N≥174 animals; 1-way ANOVA with Tukey's multiple comparison test ($p<0.0001$)], **D** day five adults [3 biological replicates; N≥118 animals; 1-way ANOVA with Tukey's multiple comparison test ($p<0.0001$)], and **E** day eight adults [3 biological replicates; N≥247 animals; 1-way ANOVA with Tukey's multiple comparison test ($p<0.0001$)]. Error bars: SEM.

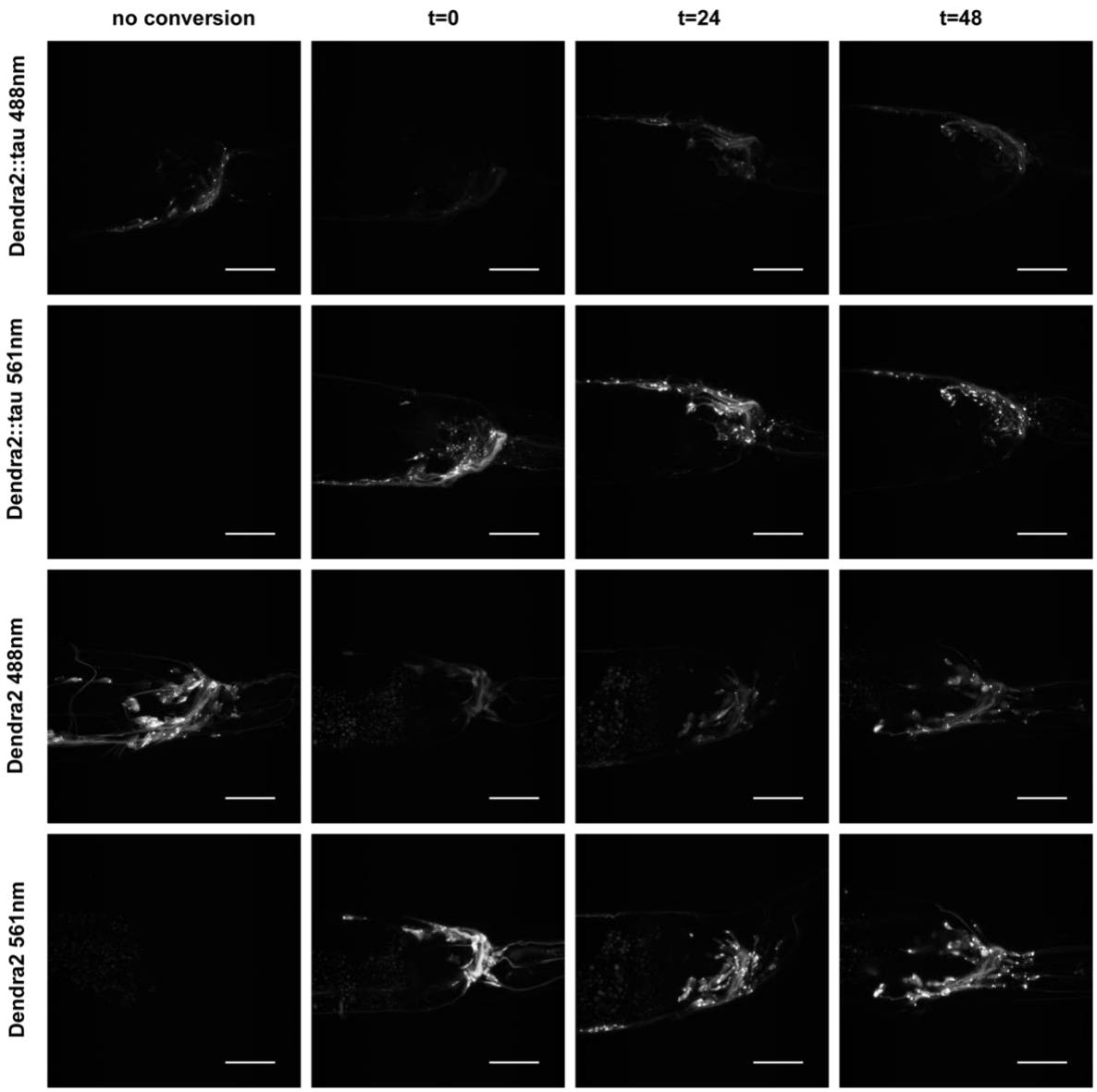

Fig. S3. Representative images of Dendra2::tau Tg M4 and Dendra2 photoconversion. Images adjusted with +40% contrast and +40% brightness. t = time in hours. Scale bar: 25μm.

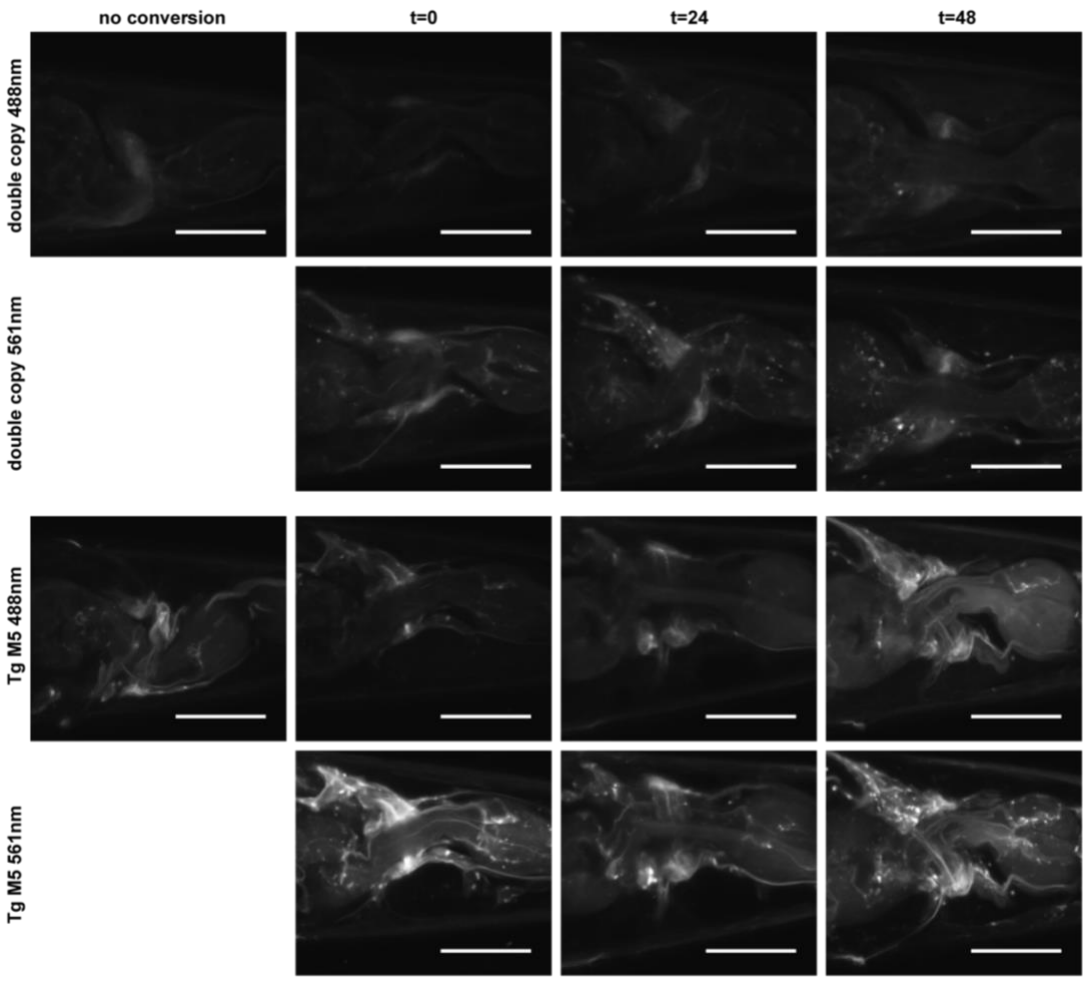

Fig. S4. Representative images of Dendra2::tau double copy and Tg M5 photoconversion. Images cropped to ROI. 561nm channel not acquired for worms that were not photoconverted. t = time in hours. Scale bar: 25μm.

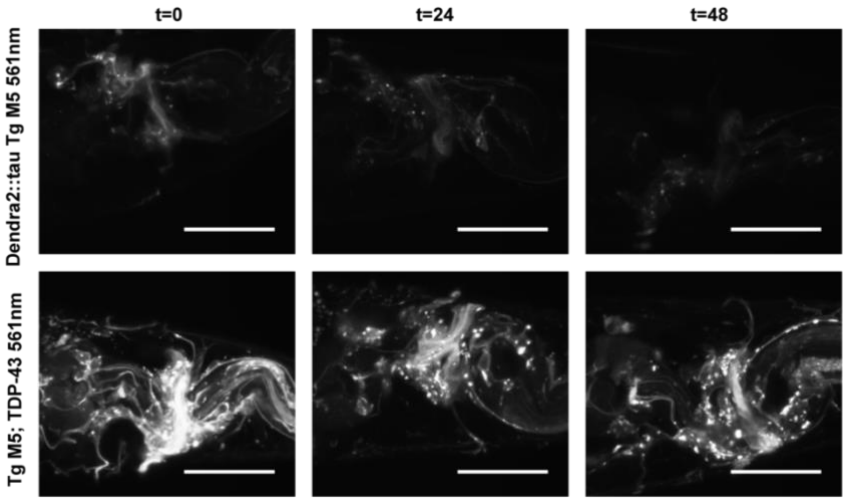

Fig. S5. Representative images of Dendra2::tau Tg M5 and Dendra2::tau Tg M5; TDP- 43 (CK402) photoconversion. 488nm channel not acquired due to green fluorescent body wall reporter of CK402. Images cropped to ROI. t = time in hours. Scale bar: 25μm.